AD-A166 759 TIME RESOLVED AND TIME AVERAGED FLOW EVALUATION FOR AN ISOLATED TRANSONIC COMPRESSOR ROTOR(U) EXOTECH INC CAMPBELL CA F NEUHOFF MAR 86 TR-0601 N00014-84-C-0766 1/1

UNCLASSIFIED F/G 20/4 NL

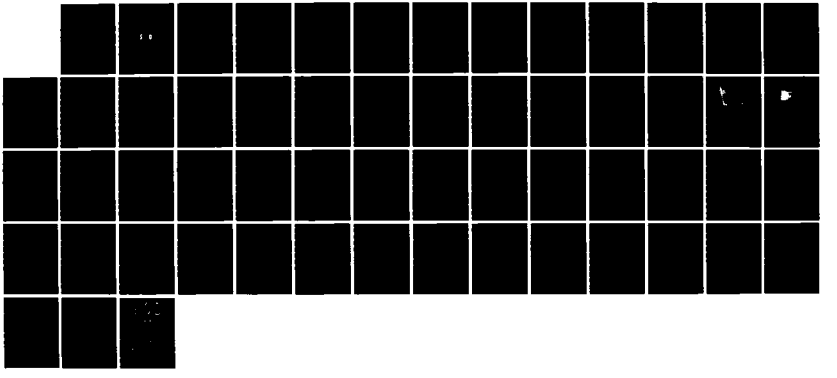

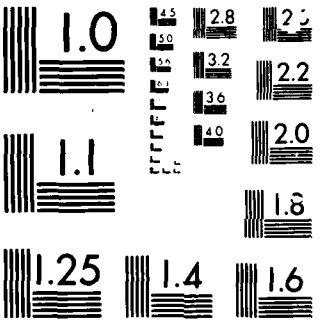

MICROCOPY CHART

exotech inc.

3rd Floor, 1901 S. Bascom Ave., Campbell,
California, U.S.A. 95008

FINAL REPORT

TIME RESOLVED AND TIME AVERAGED FLOW EVALUATION FOR AN ISOLATED TRANSONIC COMPRESSOR ROTOR.

TR 8601

MARCH 1986

PREPARED BY

F. NEUHOFF

SUBMITTED TO

NAVAL POSTGRADUATE SCHOOL,
MONTEREY, CALIFORNIA, 93943

UNDER CONTRACT

N00014-84-C-0766

UNCLASSIFIED

SECURITY CLASSIFICATION OF THIS PAGE

A166759

REPORT DOCUMENTATION PAGE

1a REPORT SECURITY CLASSIFICATION UNCLASSIFIED	1b RESTRICTIVE MARKINGS
2a SECURITY CLASSIFICATION AUTHORITY	3 DISTRIBUTION/AVAILABILITY OF REPORT Approved for Public Release; Distribution Unlimited
2b DECLASSIFICATION/DOWNGRADING SCHEDULE	
4 PERFORMING ORGANIZATION REPORT NUMBER(S) TR8601	5 MONITORING ORGANIZATION REPORT NUMBER(S)
6a NAME OF PERFORMING ORGANIZATION EXOTECH INC. / 6b OFFICE SYMBOL (If applicable)	7a NAME OF MONITORING ORGANIZATION Naval Postgraduate School
6c ADDRESS (City, State, and ZIP Code) 1901 S. Bascom Ave., Suite 337 Campbell, CA, 95008	7b ADDRESS (City, State, and ZIP Code) Monterey, CA 93943-5100
8a NAME OF FUNDING/SPONSORING ORGANIZATION / 8b OFFICE SYMBOL (If applicable)	9 PROCUREMENT INSTRUMENT IDENTIFICATION NUMBER N00014-84-C-0766
8c ADDRESS (City, State, and ZIP Code)	10 SOURCE OF FUNDING NUMBERS PROGRAM ELEMENT NO / PROJECT NO / TASK NO / WORK UNIT ACCESSION NO

11 TITLE (Include Security Classification)
Time Resolved and Time Averaged Flow Evaluation for an Isolated Transonic Compressor Rotor. (Unclassified)

12 PERSONAL AUTHOR(S)
F. Neuhoff

13a TYPE OF REPORT	13b TIME COVERED	14 DATE OF REPORT (Year, Month, Day)	15 PAGE COUNT
Final	FROM Oct 84 TO Mar 86	March 1986	53

16 SUPPLEMENTARY NOTATION

17 COSATI CODES			18 SUBJECT TERMS (Continue on reverse if necessary and identify by block number)
FIELD	GROUP	SUB-GROUP	Turbomachinery Flow Fields, Transonic Loss Measurements. Finite element Code.

19 ABSTRACT (Continue on reverse if necessary and identify by block number)

A 0.28m single stage transonic fan was operated in a rotor only configuration. Overall performance was measured and radial distributions of inlet and outlet velocity were obtained using time-averaging combination temperature-pneumatic probes. These results were compared to the prediction of a finite element computer code (TURBOFEM) prediction. The blade-to-blade velocity and pressure distributions were measured using the Dual Probe Digital Sampling technique (involving two commercial semi-conductor probes of simple design). Data were obtained from hub-to-tip at both near-sonic and at supersonic inlet relative Mach numbers. The rotor losses were derived as blade-to-blade distributions and the shock losses were evaluated as components of the total loss at each radius. Based on the limited data obtained near sonic conditions, a combination of the profile loss model of Koch & Smith and shock loss model of Dunker was found to predict the measured radial loss distribution quite well. Preliminary observations of rotor shock oscillations were also reported.

20 DISTRIBUTION/AVAILABILITY OF ABSTRACT	21 ABSTRACT SECURITY CLASSIFICATION
☐ UNCLASSIFIED/UNLIMITED ☒ SAME AS RPT ☐ DTIC USERS	UNCLASSIFIED
22a NAME OF RESPONSIBLE INDIVIDUAL R. P. SHREEVE	22b TELEPHONE (Include Area Code) (408)646-2593 / 22c OFFICE SYMBOL 67Sf

DD FORM 1473, 84 MAR — 83 APR edition may be used until exhausted. All other editions are obsolete.

SECURITY CLASSIFICATION OF THIS PAGE
UNCLASSIFIED

exotech inc.

3rd Floor, 1901 S. Bascom Ave., Campbell,
California, U.S.A. 95008

FINAL REPORT

TIME RESOLVED AND TIME AVERAGED FLOW EVALUATION FOR AN ISOLATED TRANSONIC COMPRESSOR ROTOR.

TR 8601

MARCH 1986

PREPARED BY

F. NEUHOFF

SUBMITTED TO

**NAVAL POSTGRADUATE SCHOOL,
MONTEREY, CALIFORNIA, 93943**

UNDER CONTRACT

N00014-84-C-0766

TABLE OF CONTENTS

LIST OF TABLES

LIST OF FIGURES

NOMENCLATURE

Cp	= pressure coefficient
Cpo	= pressure coefficient when aligned with flow
c_p	= specific heat at constant pressure
$\dot{m}$	= mass flow rate
M	= Mach number
N	= rotor speed
P	= pressure
S	= entropy
T	= temperature
U	= circumferential velocity component
V	= absolute velocity
W	= relative velocity
X	= dimensionless velocity obtained by dividing velocity by $V_t = \sqrt{2c_pT_t}$
α	= yaw angle
γ	= ratio of specific heats
η	= efficiency
ϕ	= pitch angle
ω	= loss coefficient

SUBSCRIPTS

A	= Type A probe
B	= Type B probe
E	= equivalent
I	= indicator for probe type
id	= ideal
R	= relative frame
ref	= referred quantity
t	= total (or stagnation) value
u	= circumferential component
v	= absolute component
o	= design value
1	= upstream of rotor
2	= downstream of rotor

I. INTRODUCTION

The work presented here reports and analyses test data acquired from a single stage axial flow compressor. The compressor was designed for supersonic rotor speeds with supersonic inlet relative flow conditions over 80% of the bladespan. Provisions were made in the instrumentation for a variety of data to be acquired. While the full range of compressor test speeds has not been attempted as yet, the compressor has proved to be a valuable tool for the development of new instrumentation and for the study of transonic flow phenomena. The testing so far has been aimed at establishing the overall stage performance map, measuring the rotor flow and developing a measurement technique that resolves all three components of the velocity vector, hub-to-tip and blade-to-blade at the rotor outlet. The latter is referred to as the Dual Probe Digital sampling (DPDS) technique and will be described in the course of this report.

In the course of the test program, rotor through-flow measurements showed that there was a significant mismatch between the rotor and the stator (Ref 1). It was concluded that the influence from one on the other would always be such that an improvement in rotor running conditions would put the stator further off-design and vice versa. This was found not to depend particularly on speed. In order to operate the rotor close to design, the stator was removed. The results given here were derived from tests of the rotor-only configuration at rotational speeds up to 22,000 RPM.

The experimental program was aimed at understanding the rotor aerodynamics as fully as possible, in particular, to determine the distribution and magnitude of losses. In the present work, the DPDS technique was applied successfully to obtain the velocity field and the rotor-relative loss

distribution everywhere at the rotor exit. The rotor losses, hub-to-tip and blade-to-blade, were compared with the predictions of loss models and published loss correlations for transonic compressor flows.

II. EXPERIMENTAL PROGRAM

II.1 TEST RIG AND INSTRUMENTATION

The compressor arrangement for the results given here is shown in Fig 1. The test rig is open loop. Ambient air enters the inlet settling chamber through a microfilter and a throttle assembly. It enters the compressor via a 0.45 m diameter duct containing a calibrated flow nozzle. From the compressor the flow is turned and exhausted radially to atmosphere. Drive power to 330 KW is provided continuously by two opposed axial air turbine stages powered by the Laboratory air supply. The rotor was designed for a relative inlet Mach number of 1.5 at the tip, at a speed of 30,460 RPM. The hub-to-tip radius ratio is 0.5 at the inlet and 0.655 at the outlet with a constant outer radius. The rotor design is given in Ref 2. The blading is double-circular-arc but with the pressure side flat.

The instrumentation can be divided into four catagories; namely, fixed instrumentation for blade row performance measurements, radial survey probes, case wall static pressure tappings and high response (Kulite) transducers with associated computer software.

The blade row performance instrumentation included individual probes for stagnation temperature and pressure in the inlet, a distributed rake of 20 kiel probes and 3 temperature probes in the exit annulus and the flow nozzle measurement of flow rate.

Four-hole combination pressure and temperature probes (Fig 2) can be traversed radially at measuring stations 0, 1 and 2. The probes are

calibrated as described in Ref 3 to give the time averaged velocity vector, total and static pressures. At high inlet velocities the probe at station 1 is removed since the wake could excite vibrations in the rotor. The inlet conditions at station 1 are then inferred from measurements at station 0, using the now-established knowiedge of the flow between these two stations.

Static pressure tappings in the compressor case wall cover a region starting 2 chord lengths ahead of the leading edge and ending 1.5 chord lengths behind the trailing edge of the rotor. Other taps are located on the compressor hub just behind the rotor trailing edge.

Kulite transducers used in conjunction with a high speed digital data acquisition system provide two types of measurement, namely, unsteady case wall pressures and the time-resolved rotor exit velocity vector distribution. A computer-controlled sampling technique that allows the data to be taken at specific predetermined positions with respect to the rotor independent of rotor speed is used in both cases (Ref 4). Twelve wall pressure transducers are positioned between 0.5 chord length up and down stream of the rotor. The positions are such that there are pneumatic taps at the same axial locations, but circumferrentially displaced. Blade-to-blade distributions of static pressure are acquired with sufficient resolution to resolve shock locations within the blade passages .

The time resolved velocity vector measurements involves two Kulite probes positioned in the annulus downstream of the rotor and used in a method referred to as the dual probe digital sampling (DPDS) technique.

II.2 DPDS TECHNIQUE

The technique is described in detail in Ref 4 and only a brief summary of the principles will be given here. At measuring station 2 (see Fig 1 and 3),

two probes of different design (Type A and Type B) are mounted circumferentially separated on the case wall such that they can be translated radially and also rotated around their tips. The probe outputs are sampled at the same point in the rotor frame of reference (at delayed times) with the probes set to nine angles with respect to their axes. A procedure analogous to the calibration procedure used for multi-sensor probes is applied to the dual probe system to derive Mach number and flow angles from the two arrays of 9 measurements.

The Kulite transducers in the probe tips are protected by perforated steel caps which enclose an internal volume of approximately 0.10 mm^3. In contrast to the probes described in Ref 4, the present caps have holes which are oriented in straight lines across the front face arranged parallel to the probe shaft for the Type A probe and perpendicular to the probe shaft for the Type B probe (Fig 4). Due to the different design of the two probes, their dependence on Mach number, pitch and yaw angle is quite different. In Fig 5a the output of the Type A probe is shown for one Mach number and a range of pitch and yaw angles. The probe is quite insensitive to pitch angle, strongly but symmetrically dependent on yaw angle. The magnitude of the output increases with Mach number. Fig 5b shows the Type B probe for the same range of conditions. The strong dependence on pitch angle shown was found at all Mach numbers. Therefore, while the Type A probe is a good indicator of the Mach number, and independent of pitch angle, the Type B probe provides means to measure the pitch angle. In Ref 5 the use of the probe data in the calibration and actual tests is described in detail. The specific characteristics of these probes made some changes necessary. While a Type B probe of the former design has a clear maximum in its output versus probe yaw angle curve when the probe is aligned with the flow, this probe does not have this feature. Fig 5b shows that for a given Mach number the probe will have a

maximum reading at various yaw angles for different pitch angles. Also, it was found that variations in Mach number changed yaw angle corresponding to the maximum output. These variations did not appear to be regular in nature. In an actual test the probe yaw angle corresponding to the maximum output of the Type B probe was taken as the actual flow yaw angle. This was no longer possible for the new type probe. From the data shown in Fig 5 only four values are required to establish a calibration for the two probes as system: namely, the maxima in the output of the Type A and Type B probes and the values of the Type A probe corresponding to two readings 110° in yaw angle apart. These latter two values are the same. The center value of the two angle readings ideally would be the flow yaw angle, if the probe would be symmetrical in yaw angle. The calibration showed, that the center of the 110° yaw angle spread disagreed with the flow yaw angle between 1 and 2°. The disagreement depended little on pitch angle but was well behaved with Mach number. Higher speeds seem to improve the probe characteristics. A low order polynominal was used to express this Mach number dependence (Fig 6). Once the Mach number is established in the probe's application, the yaw angle can be corrected using this polynominal. The four values are treated like the pressure readings from a conventional four (or five) hole pneumatic probe. Two pressure difference coefficients are defined which depend on Mach number and pitch angle. The calibration is represented as surfaces of Mach number and pitch angle as functions of the two coefficients, using polynomials in two variables (Ref 3).

Another difference to the former probes of other tip geometry was observed. While the Type A probe read the correct total pressure as long as the pitch angle did not exceed -5° and +15°, the new Type A probe is more sensitive to pitch angle variations. In Fig 7 the dimensionless pressure coefficient $C_{P_{oA}}$ averaged for all Mach numbers is plotted against flow pitch angle.

$C_{P_{oA}}$ is the ratio of the difference between Type A probe reading at an aligned (yaw) position and the static pressure over the dynamic head. For fairly small pitch angles (8° or more) the value of $C_{P_{oA}}$ starts decreasing noticeably. However, $C_{P_{oA}}$ is well behaved with pitch angle and is represented by a fourth order polynominal.

In application in the compressor, the two arrays of nine measurements (obtained at each point in the rotor frame by rotating the two probes to nine yaw angles varying from -60° to +80° about the time averaged value read from the combination probe), are reduced in turn to obtain the local flow yaw angle, Mach number and pitch angle. First, using curve fitting to the Type A probe data, the probe flow yaw angle is obtained as the mean of the probe settings which are calculated to give a spread of 110° between similar values of the probe output. The similar values for the 110° spread and the maxima of the Type A and Type B probe outputs are also obtained by curve fitting, and the two pressure difference coefficients are then calculated. The local Mach number and pitch angle are obtained using the polynomial surface approximations to the calibration data. Using the obtained value of Mach number the flow yaw angle is corrected (Fig 6). The flow pitch angle is used to determine $C_{P_{oA}}$ which in turn is used to calculate the correct total pressure from the Type A probe. The accuracy of the measurement is discussed in Appendix A.

II.3 TEST PROGRAM

Tests were run at open throttle between 50% and 70% of design speed, blade row performance data and wall Kulite transducer data were recorded at selected speeds.

At 70% speed, radial surveys of twenty measurements were made using combination probes at stations 0 and 2. Five samples were recorded for each

measurement. At the same operating conditions, the DPDS technique was applied at five radial stations at the rotor exit; namely, 26, 42, 50, 74 and 90 percent of the blade span from the hub. Data were acquired at 256 positions across two adjacent blade passages. The combination probe data were reduced to give radial distributions of the time averaged velocity vector, stagnation pressure and temperature. The DPDS data were reduced to give blade-to-blade distributions of velocity vector at the five radial positions. Distributions of stagnation pressure and temperature, and losses were also deduced.

Additional tests were run when periodic oscillations at frequencies much higher than blade-passing frequency were observed on an oscilloscope output monitor of selected wall Kulite transducers. The rotor speed was varied from 66% to 70% speed in eight steps while the blade-passing and high oscillation frequencies for one transducer were obtained using a frequency analyser online.

III. RESULTS

The results given here were achieved in various test runs at different times. They are, however, presented in groups of common subjects so that a logical order can be maintained.

III.1 TIME-AVERAGED FLOW

In Ref 1 it is shown, that the flow rate achievable at a full open throttle is not sufficient to allow the correct incidence angle over the whole blade span. Since throttling will only reduce the flow rate, the rotor in flow would get worse. Thus no attempt has been made to establish a compressor performance map as such. For a unthrottled configuration the blade row performance was measured at various speeds (Tab I). In order to be able to predict the performance for higher speeds and to put the measured performance into perspective to individual speed lines, the performance map of this rotor

was calculated. The through flow code used was the finite element Q3DFLO-81 code of Hirsch (Ref 6 and 7). Fig 8 shows the mesh used for the calculation with the location of the rotor indicated. The performance map (Fig 9) was calculated for a speed range from 50 to 100%. Measured data (Tab I) is plotted as well. While the measured efficiency agrees rather well with the calculated adiabatic efficiency, the measured total pressure ratio is slightly lower than the calculated one. For maximum efficiency the adiabatic efficiency does not depend very much on speed, while the pressure ratio changes substantially. Since the speeds at which measurement data is available do not match the calculated speeds exactly, this is looked at as a possible explanation for the total pressure ratio discrepancy. The measured flow rates, however, approximate those for the calculated peak efficiency rather well. Hence it is assumed , that the rotor, if operated at open throttle, performs very close to its best operating condition. The results of the combination probe surveys were used to derive the rotor-relative flow conditions, which are required for an evaluation of blade-to-blade losses. Of particular importance are the relative Mach number and incidence angle which determine the passage shock position and strength.

A comparison was made with flow code predictions for the given compressor geometry, test speed and measured flow rate. Results for rotor in-and outlet conditions are shown in Fig 10 through 13. Good quantitative agreement is seen between measured and calculated inlet flow and good qualitative agreement is found in the outlet flow. While the relative Mach number reached unity only at the tip, it exceeded 0.8 over more than 50% of the blading.

The incidence angle to the rotor blading is shown in Fig 14. Again, the agreement between measurements and code predictions is qualitatively excellent and quantitatively good. Also shown in Fig 14 is the code prediction of the

optimum (design) incidence angle for the given blading. Clearly, in the hub region the incidence angles are larger than they should be, for reasons discussed in Ref 1 and 8. Over the outer 50% of the blading the measured incidence angles were within 2° of design.

III.2 DPDS MEASUREMENTS

The DPDS technique determines the three dimensional velocity vector in the absolute frame; this includes a determination of the pitch angle, (which is not normally available from LDV or L2F measurements). The rotor exit flow from DPDS measurements is shown blade-to-blade and hub to tip in Fig 15.

From these quantities the rotor outlet relative Mach number (Fig 16) and relative flow angle β_2 (Fig 17) were derived. While the Mach number varies as is characteristic for a blade wake, the flow angle is not, as assumed so far, constant peripherally. Indeed rather large changes occur in the blade wake.

The variation of pitch angle through the wake appears to be quite large and hence the applicability of two-dimensional cascade flow concepts would initially be suspect. However, if the pitch angle is calculated in the relative system, it is found to have only about half of the magnitude in the absolute system. This is important if a comparison of rotor-relative loss measurements with two-dimensional steady cascade data is to be meaningful. The rotor-relative losses can be calculated from the DPDS measurements since the DPDS technique determines the total pressure as well as the velocity vector. The loss coefficient $\bar{\omega}$ for a blade element is defined as (see Appendix B)

$$\bar{\omega} = \frac{\bar{P}_{t2Rid} - P_{t2R}}{\bar{P}_{t1R} - \bar{P}_1} \qquad (1)$$

For the rotor, assuming that the inlet flow is axisymmetric, $\overline{P}_{t2Rid}$, $\overline{P}_{t1R}$ and $\overline{P}_1$ are constant values derived from combination probe data and only P_{t2R}, the relative total pressure at the rotor outlet, varies circumferentially. The derivation of P_{t2R} from quantities measured in the absolute frame is given in Appendix B. The calculation of P_{t2R} and $\overline{\omega}$ was carried out for the DPDS data at the five radii measured and the result is shown in Fig 18. At 26% span the blade wakes are rather wide, probably due to an incidence angle of 6°. At larger radii (>55% span), the region between two blade wakes ceases to be loss free. At these locations, from Fig 11 it can be seen that the relative inlet Mach number is 0.85 or larger. Since this exceeds the critical Mach number, it is required that a shock be present in the passage. In Refs 9 and 10 it is proposed that such a shock will produce a loss, that rises gradually from its lowest value at the pressure surface to its highest value at the suction surface. In this inviscid model, in the region of the blade wake, a discontinuity between suction surface and pressure surface values would occur. The increase in loss from pressure to suction surface is largely the result of the increase in Mach number due to the acceleration of the flow over the suction surface. This simple model appeared to explain the trends in the measured losses quite well. In order to obtain values for the shock loss from the measurements, the loss distribution outside the wake was approximated with a first order polynominal. The center of the wake was determined from the blade-to-blade distribution of relative outlet Mach number (Fig 16) and the point where the pitch angle changed through the time averaged value from the highest to the lowest value. Using a linear approximation the shock losses were integrated at each of the radii where supercritical conditions occured.

Also, to obtain the total loss at each radius, the relative outlet total pressure, P_{t2R}, was mass-averaged circumferentially and used in Equ (1). The

radial distributions of shock and total losses derived from the DPDS measurements, are shown in Fig 19. The total losses calculated from combination probe surveys are also included in Fig 19.

III.3 HIGH RESPONSE WALL STATIC PRESSURE MEASUREMENTS

Fig 20. shows an oscilloscope trace from one high response wall static pressure transducer. The transducer was located at about mid chord. Imposed on the dominant blade passing frequency is an oscillation which varies in amplitude depending on the particular blade passage. The oscillation occured at a transducer and at a blade-to-blade location which suggested that it originated from the passage shock. The results obtained from the frequency analyzer showed that the oscillation frequency was some twenty times as large as the blade passing frequency. The variation of the oscillation frequency as the rotor speed increased is shown in Fig 21. It is noted that as the speed was increased, a larger number of blade passages and different transducers through the rotor passage exhibited the high frequency oscillation. Also the oscillation amplitude appeared to increase with speed. While the frequency is too high for structual response to be a concern, the Strouhal number based on relative velocity magnitude and blade thickness at the tip is between 0.1 and 0.2. Thus, shock oscillation coupled with vortex shedding is a probable mechanism.

Assuming that the oscillation was caused by a high frequency movement of the passage shock, an approach proposed in Ref 11 and Ref 12 was followed to calculate the losses which would result from the oscillation. An increase in losses will result from shock oscillation since the increase of entropy rise across a shock is not linear with increasing Mach number and thus, if the Mach number varies about its mean value (due to relative motion), the increase in entropy rise for the high relative Mach number will be larger than the abso-

lute value of the decrease in entropy rise for the low relative value. This produces a larger entropy rise than would be produced by a steady shock at the mean Mach number. Shock oscillation amplitude and frequency as well as mean value of Mach number are therefore the parameters which determine the magnitude of the losses. For the present test conditions, it was found, that due mainly to the low inlet Mach number (~1.04) the losses from the observed shock oscillation would be negligibly small.

IV. ANALYSIS OF THE LOSS MEASUREMENTS

Many attempts have been made to correlate data for losses measured in compressors using models which identify and sum various loss components. Influenced largely by the conclusions of Ref 13, the losses obtained in the present study have been compared with values derived from the work of Lieblein (Ref 14), Dunker (Ref 15), Swan (Ref 16) and Koch & Smith (Ref 17). It is noted that the correlations used are for cascade flows. Since in the compressor, the pitch angle relative to the rotor was measured to vary peripherally no more than +/-7° through the blade wake, a comparison with cascade correlations is appropriate.

The measurements resulted in data for the shock loss and the total loss as a function of radial position (Fig 19). In order to isolate shock loss from the total loss, an extrapolation of the inviscid flow behavior to a discontinuity in the blade wake was required. Clearly, integration of the viscous wake profile when shocks are present in the outer flow gives a loss which is partly profile loss and partly shock loss. Thus the profile loss cannot be identified separately from the measurements. The profile losses which would be expected from the off-design correlations of Lieblein (Ref 14) were examined. From the combination probe measurements of inlet and outlet velocities and the known blading geometry, the equivalent diffusion factors, wake

momentum thicknesses and hence profile losses were calculated for each stream surface following Ref 14. Since the correlation for wake momentum thickness versus equivalent diffusion factor involves an uncertainty band, a possible range for the profile losses is calculated. The results are shown in Fig 22. Also shown in Fig 22 are the profile loss values which result when two different through-flow computer codes were applied to the rotor geometry. The finite-element code Q3DFLO-81 incorporated the loss correlations of Koch & Smith (Ref 17). The computer code FVVOFF incorporated the profile loss correlations of Swan (Ref 16). The latter results were taken from Ref 18. They are seen to depart significantly from the qualitative variation expected from the other two. Since the center section of the blade was operating closest to optimum incidence, the higher profile losses given by the FVVOFF are suspect.

The shock losses deduced from the blade-to-blade measurements were compared with the predictions of shock losses incorporated in the computer programs Q3DFLO-81 and FVVOFF. The result is shown in Fig 23. Q3DFLO-81 utilizes the method of Koch & Smith (Ref 17) which analyses a simplified model of the flow incorporating profile leading edge geometry. The Mach number and leading edge thickness are the most influential parameters in this model. The model predicts no shock loss for the present test conditions except at the blade tip. A more elaborate shock loss model developed by Dunker (Ref 15) is incorporated in program FVVOFF. Similar to Moeckel (Ref 19), the model considers a bow shock ahead of and a normal shock across the blade passage to the suction surface of the next blade. The position and strength of the shock, and therefore the losses depend on inlet Mach number, angle and rotor geometry. The agreement between the prediction with this model and the measurements is seen in Fig 23 to be very good.

Since the blade-to-blade flow measurements support the modeling of the flow as being cascade-like out to 80% of the span, it is appropriate to compare the total loss measurements with predictions for the sum of profile and shock loss components. This is shown in Fig 24, where the profile loss is that of Koch & Smith and the shock loss that of Dunker. The agreement is seen to be quite good. Whether similar agreement will be found at higher transonic speeds, or whether stronger three-dimensional effects will be found, will be determined in future tests.

V. CONCLUSIONS

An axial compressor rotor was operated at moderate transonic inlet conditions and the rotor flow field was examined at inlet and outlet. All components of the outlet velocity vector were determined at 256 points, blade-to-blade, across two identified blade passages at each of 5 radial positions. The losses in the rotor frame of reference were derived as blade-to-blade distributions and the shock losses were evaluated as components of the total loss at each radius . Based on the limited data obtained to sonic relative Mach numbers at the tip, the flow remained cascade-like through the rotor without strong three-dimensional or case wall effects to 80% span. A combination of the profile loss model of Koch & Smith and shock loss model of Dunker was found to predict the measured loss distribution quite well. Measurements at higher rotor speeds are now required to examine the validity of the loss models over a range of Mach numbers and to investigate whether or not stronger three-dimensional effects are developed. The capability of the DPDS technique to resolve the radial as well as tangential and axial velocity components of the velocity, including within the rotor wakes, was verified.

TABLE I

OVERALL COMPRESSOR PERFORMANCE

$\frac{N_{ref}}{N_o}$ [/]	0.395	0.493	0.524	0.556	0.589	0.620	0.654	0.687
$\dot{m}_{ref}$ [Kg/s]	4.000	4.981	5.293	5.677	5.980	6.243	6.575	6.867
$\frac{P_{t2}}{P_{t1}}$ [/]	1.058	1.093	1.105	1.120	1.133	1.148	1.166	1.181
η[%]	88.6	91.3	90.7	91.6	91.3	92.7	92.6	90.4

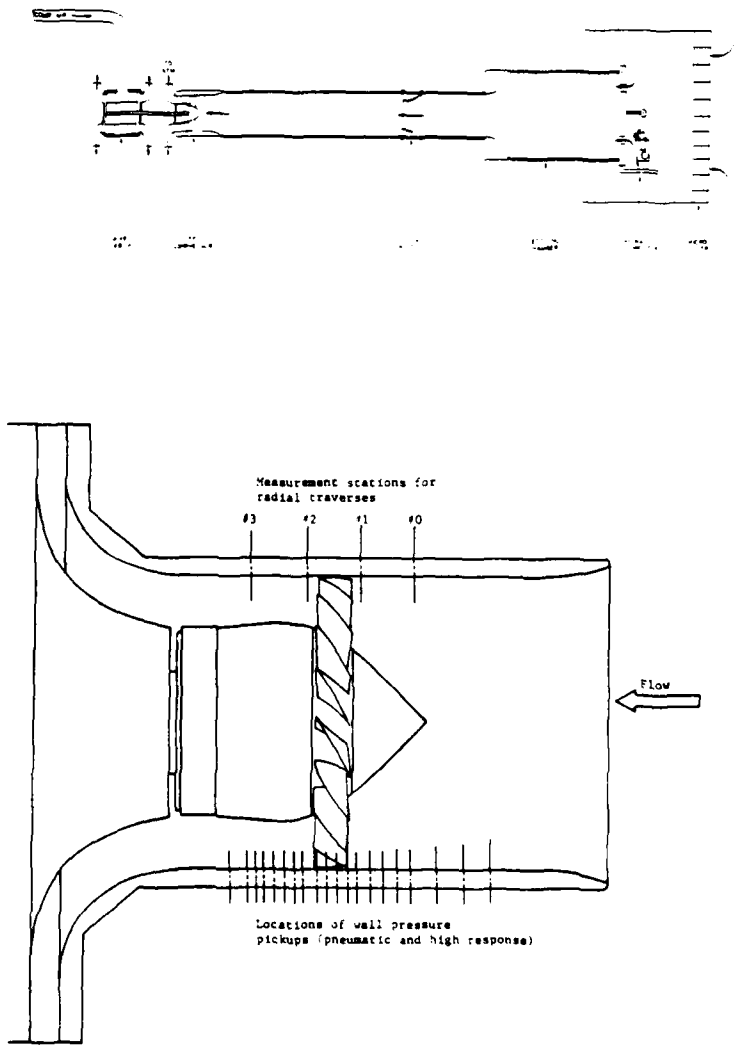

Figure 1. Compressor Test Rig and To-Scale Drawing of Test Configuration

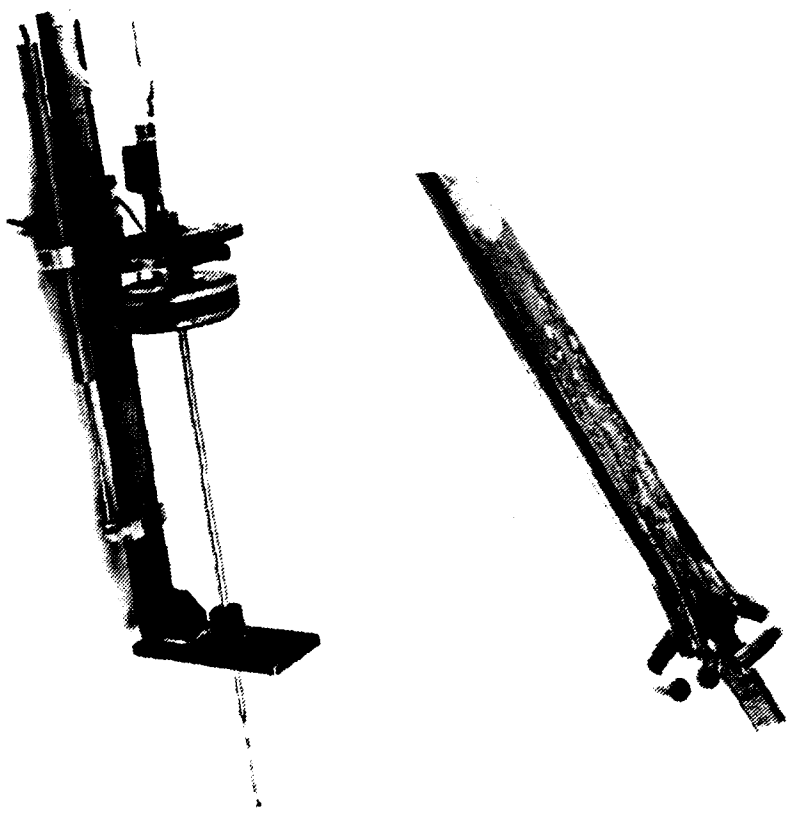

Figure 2. Combination Temperature-Pneumatic Survey Probe

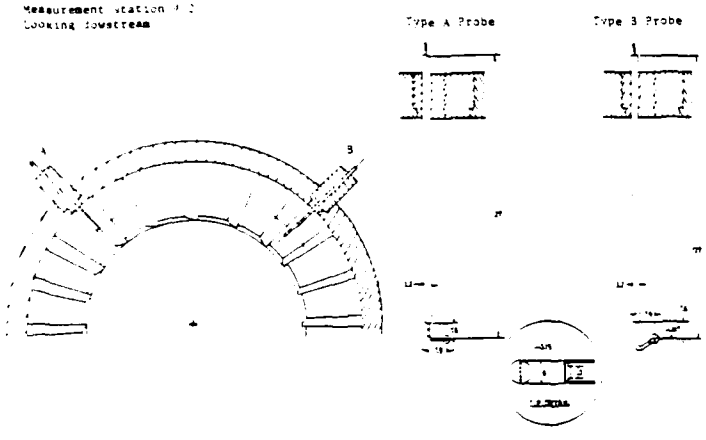

Figure 3. DPDS Instrumentation

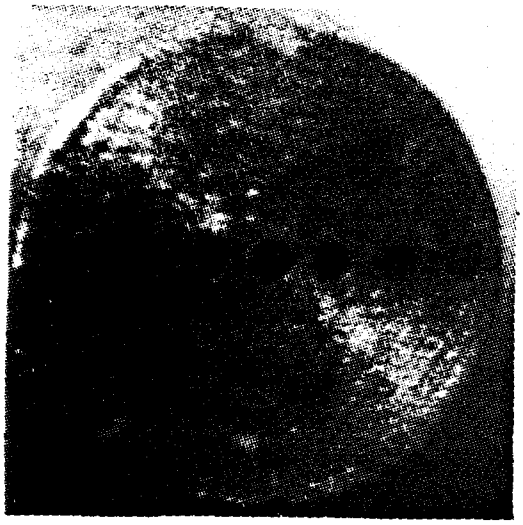

Figure 4. View of Kulite Probe Tip Geometry

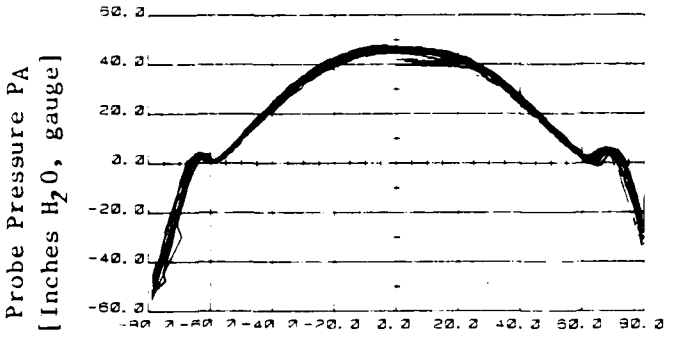

(a) Type A Probe

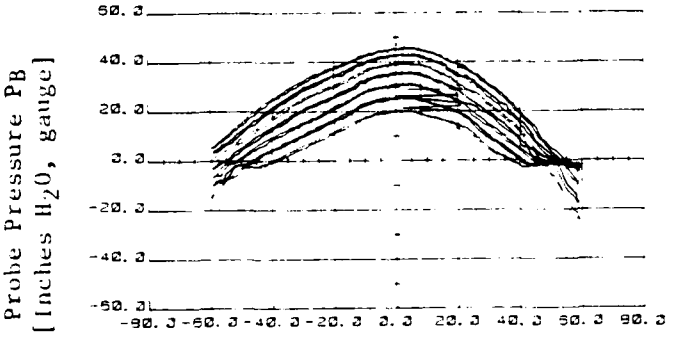

(b) Type B Probe

Kulite Probe Calibration at Constant Mach Number (0.4) and seven Pitch Angles from -4 degrees to +20 degrees

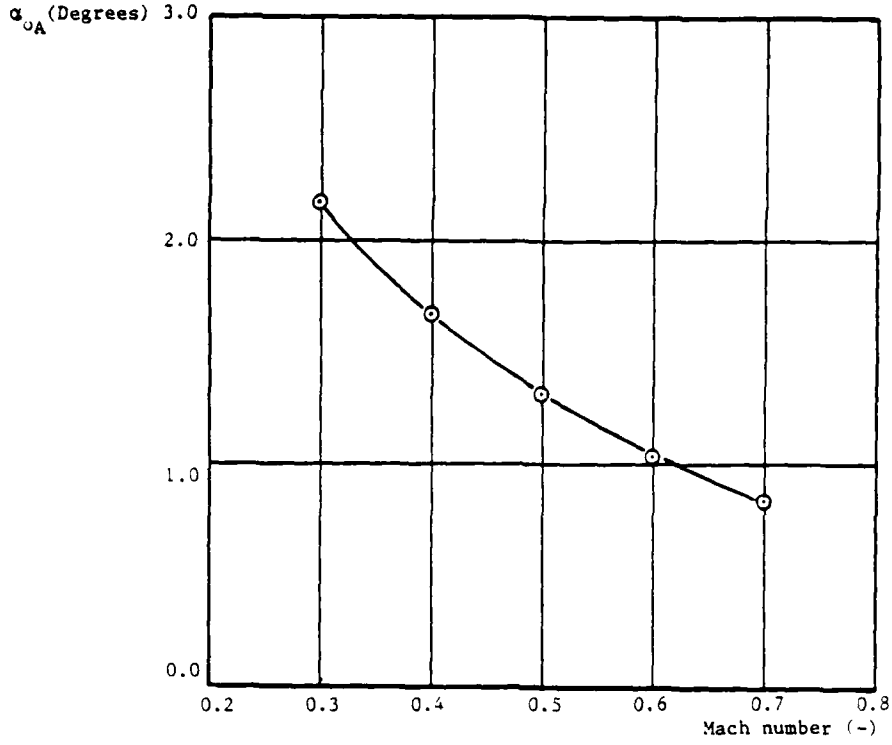

Figure 6. Type A Probe Flow Yaw Angle Correction

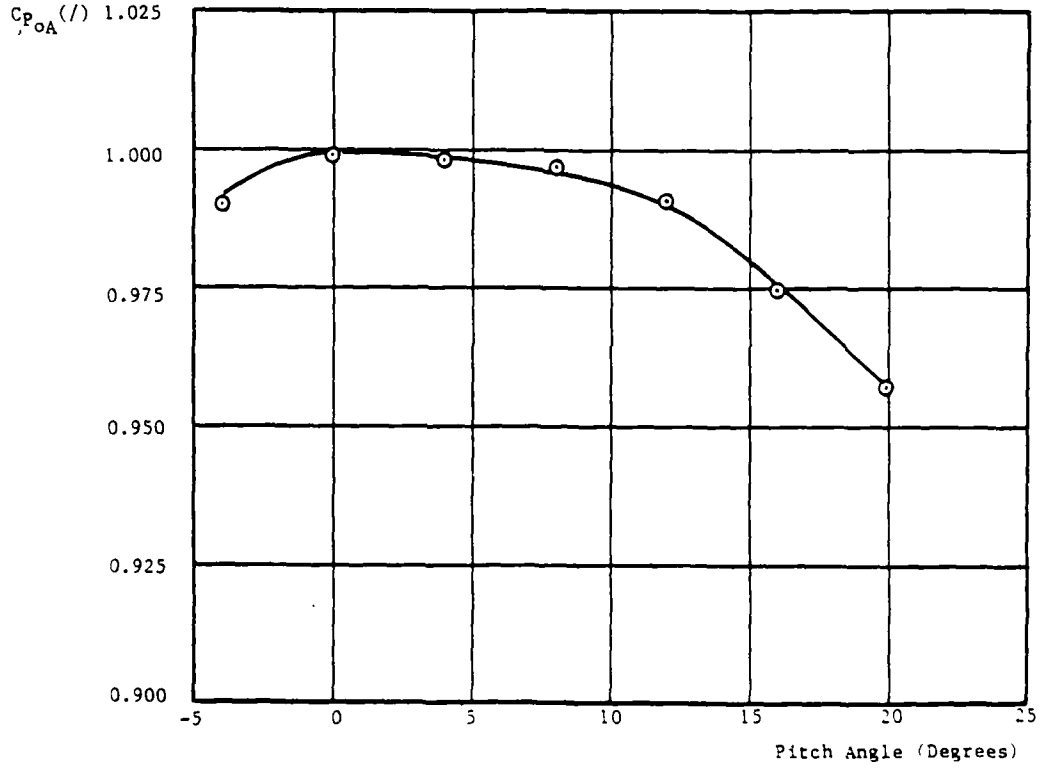

Figure 7. Zero Yaw Angle Pressure Coefficient of the Type A Probe versus Pitch Angle

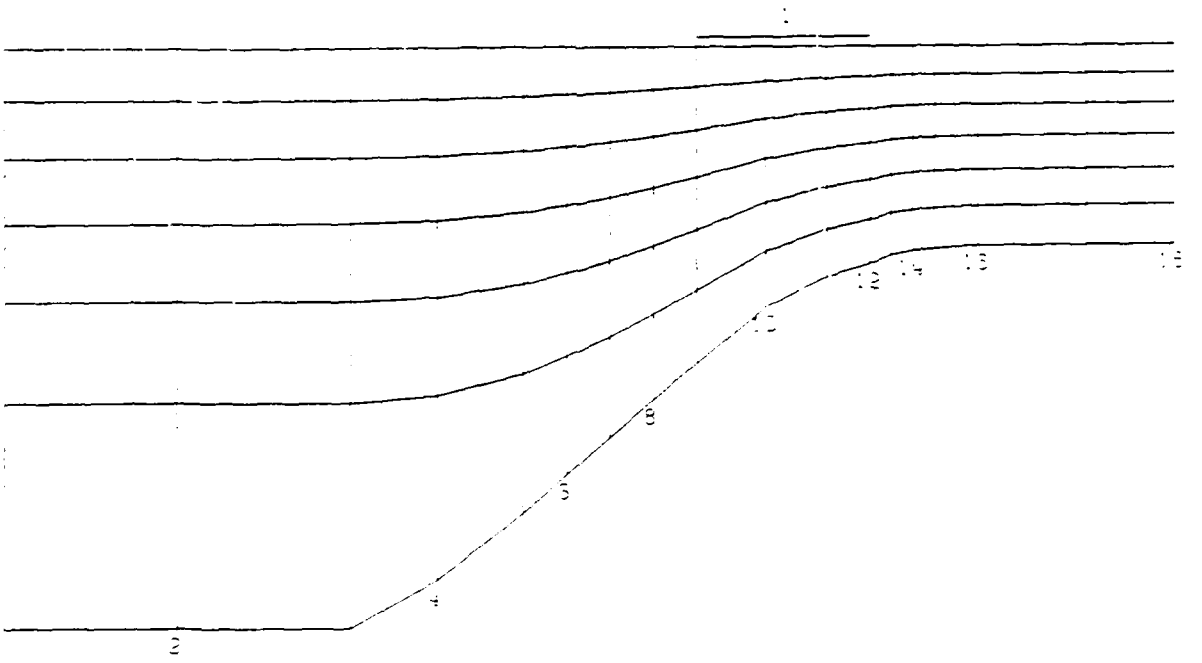

Figure 8. Finite Element Mesh of Through Flow Calculation

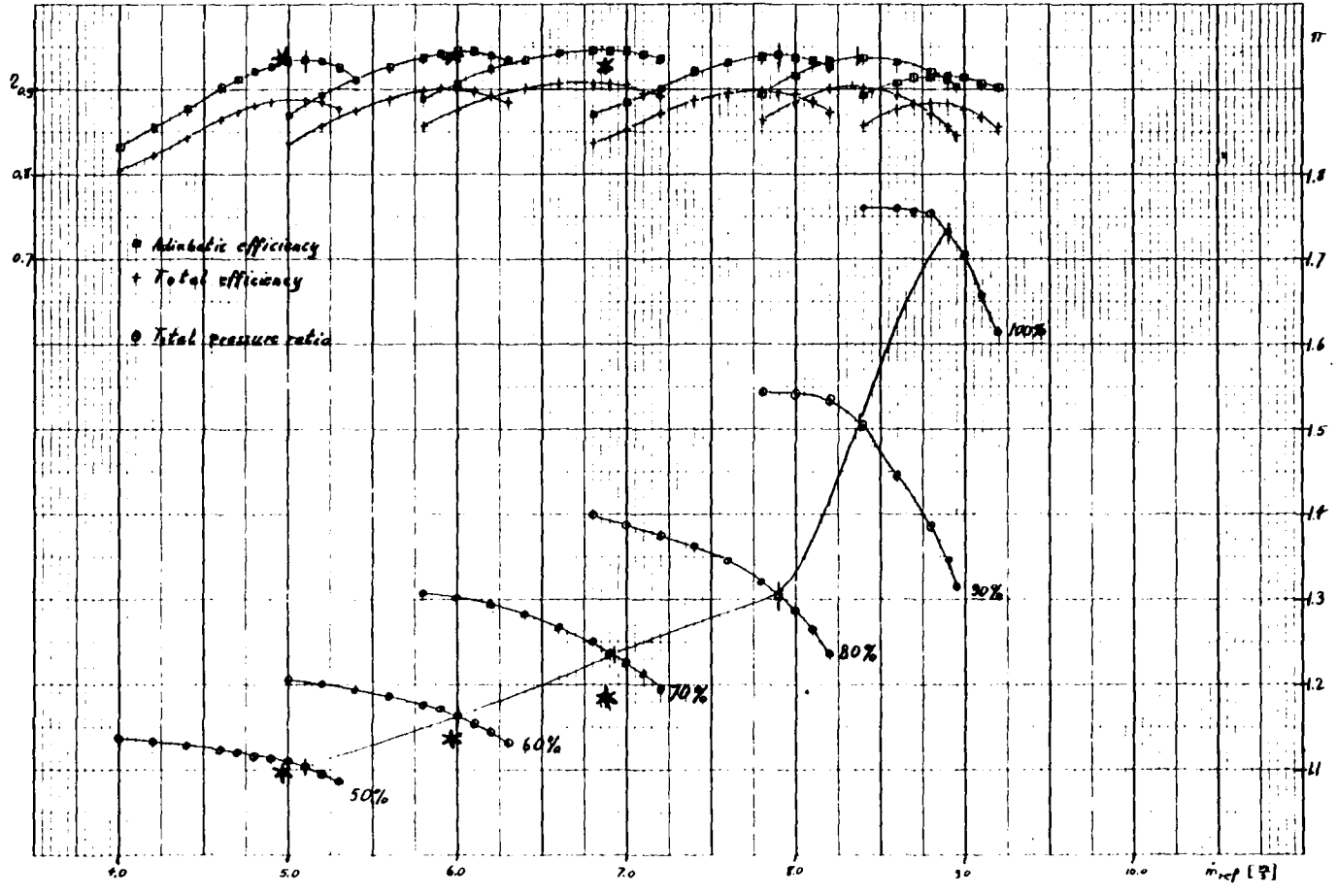

Figure 9. Calculated Performance Map (* - Measured Values)

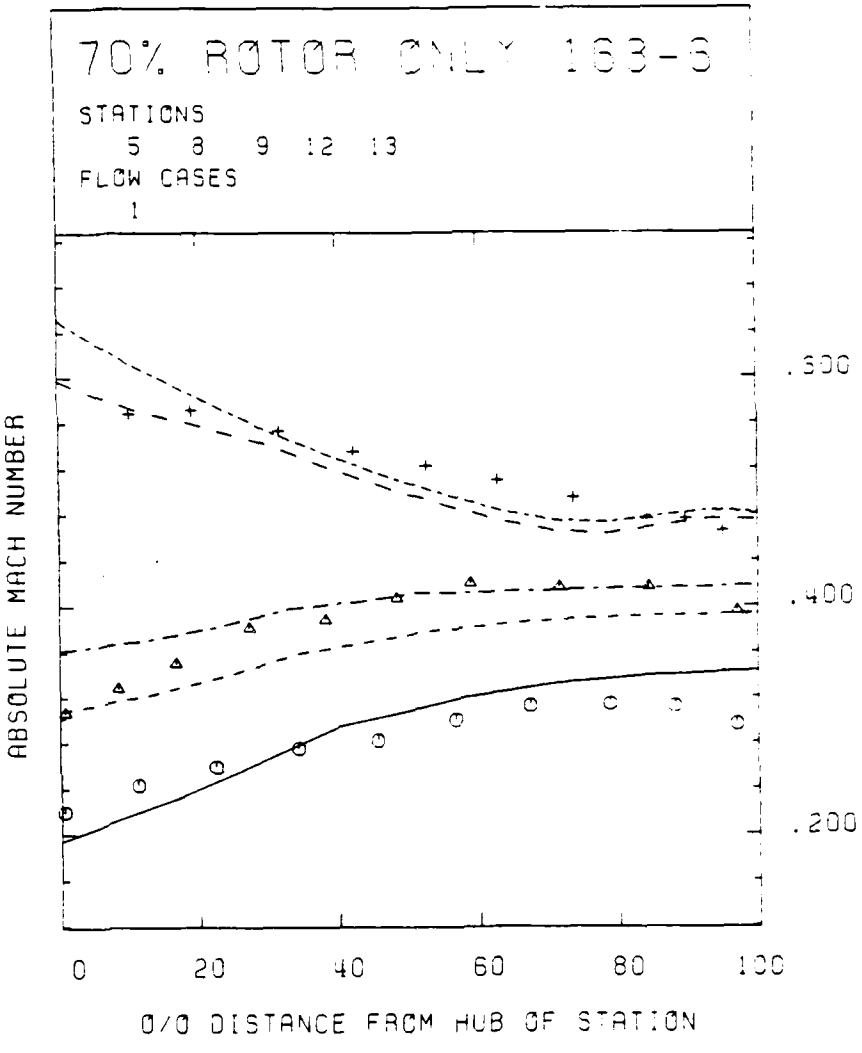

Figure 10. Absolute Mach Number at Various Axial Locations

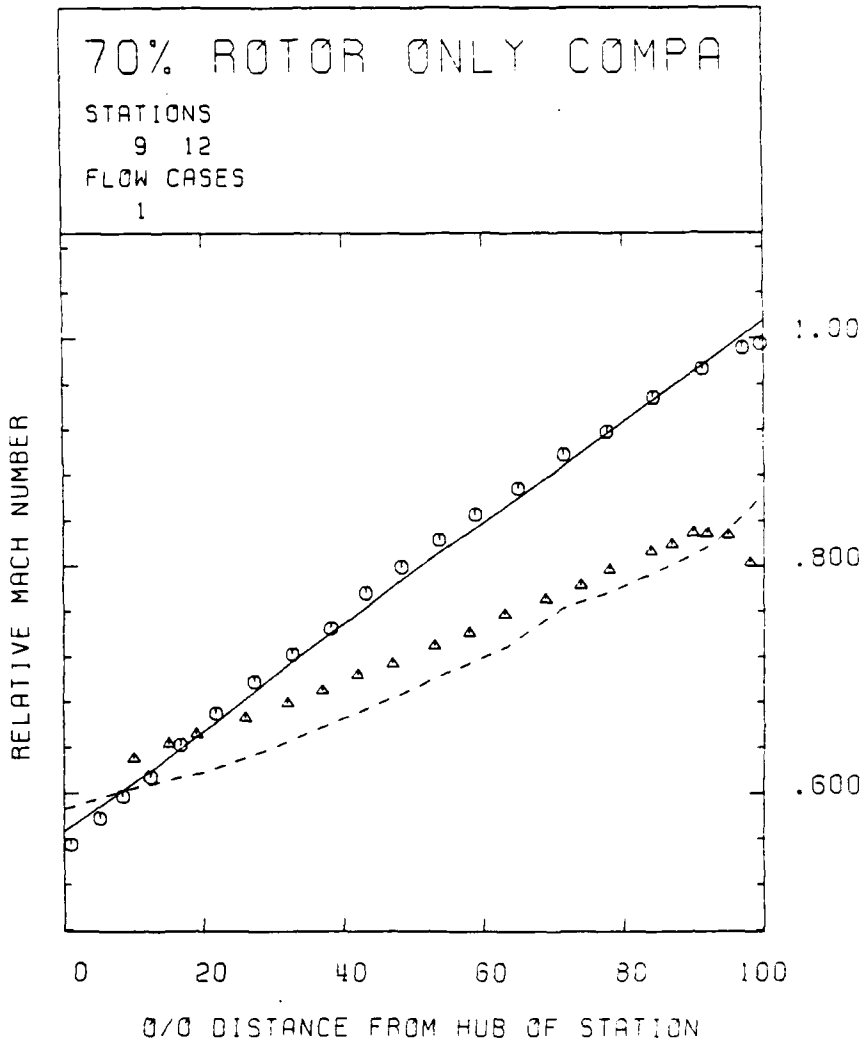

Figure 11. Relative Mach Number at Rotor Inlet and Outlet

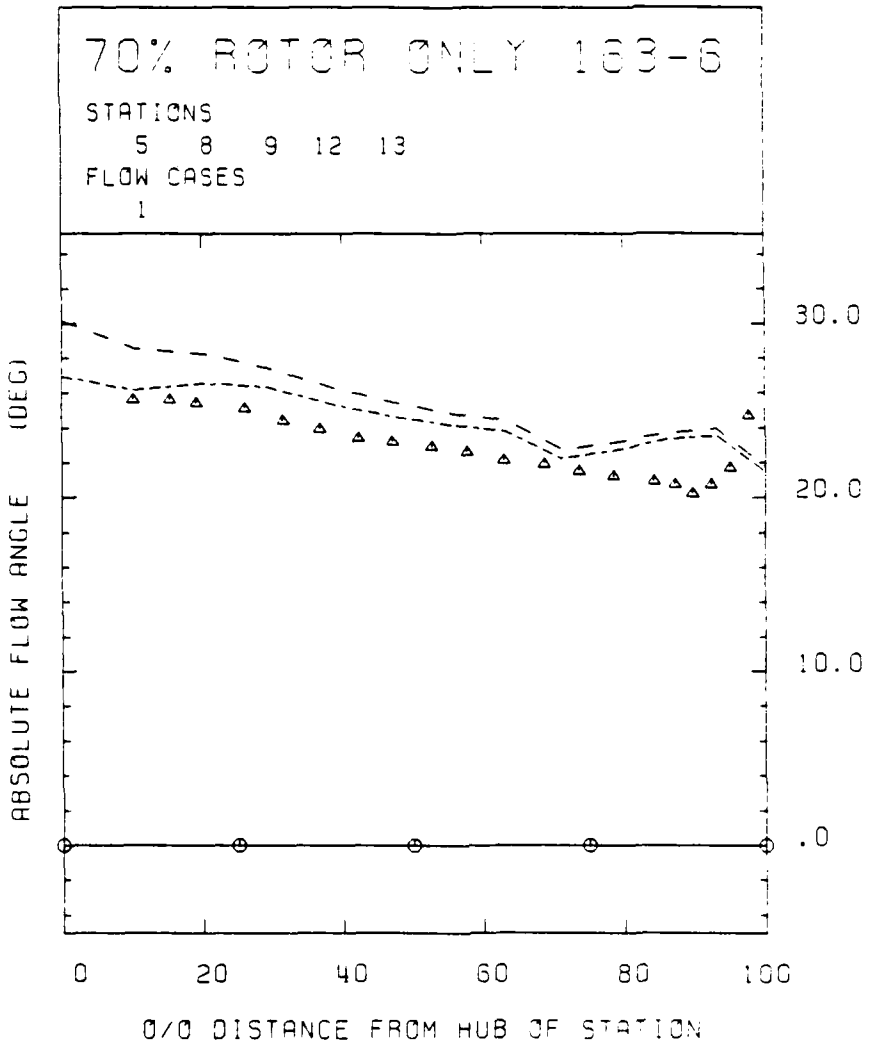

Figure 12. Absolute Flow Angle Hub-to-Tip at Rotor In- and Outlet

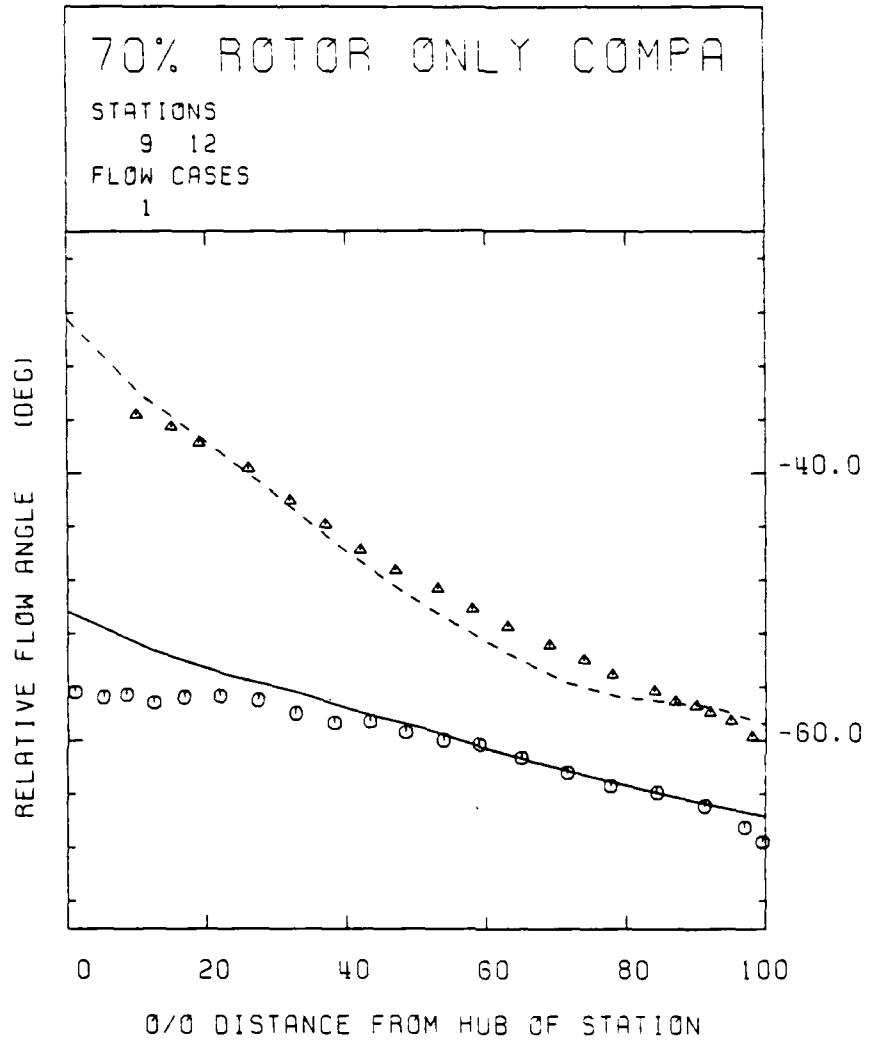

Figure 13. Relative Flow Angle Hub-to-Tip at Rotor In- and Outlet

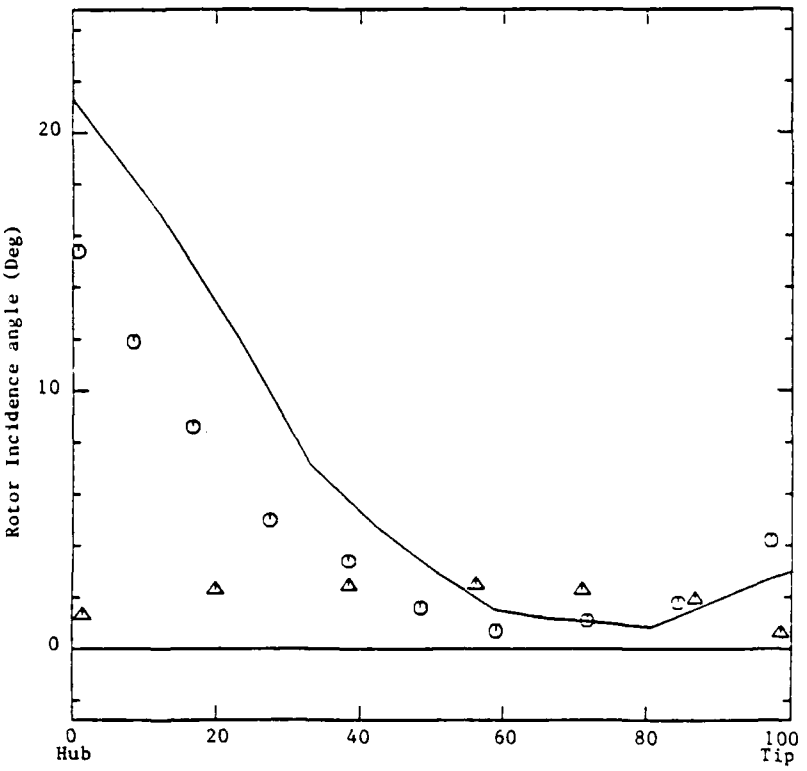

Figure 14. Flow Incidence at the Rotor Leading Edge

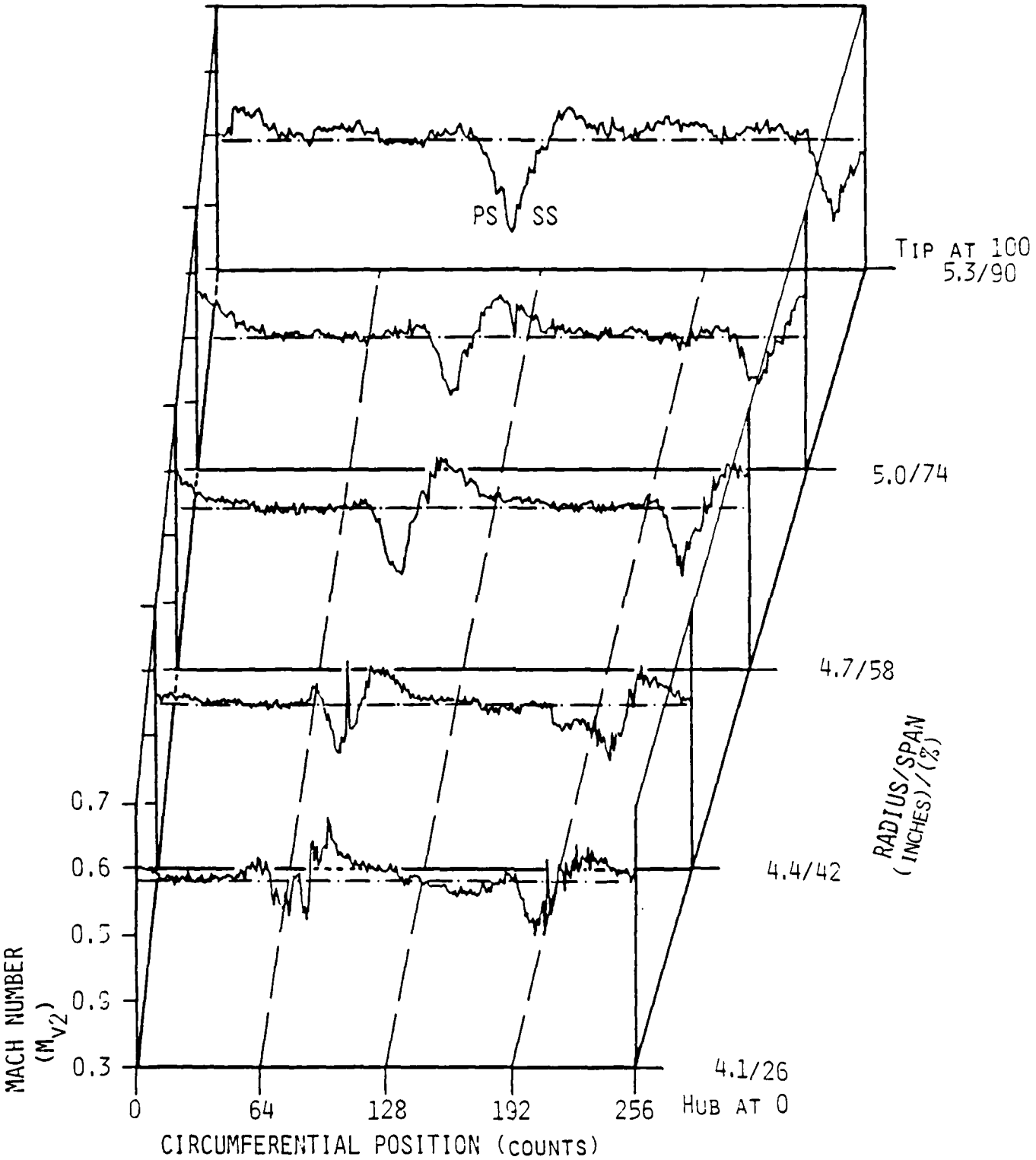

Figure 15a. DPDS Measurements of Blade-to-Blade Flow Mach Number

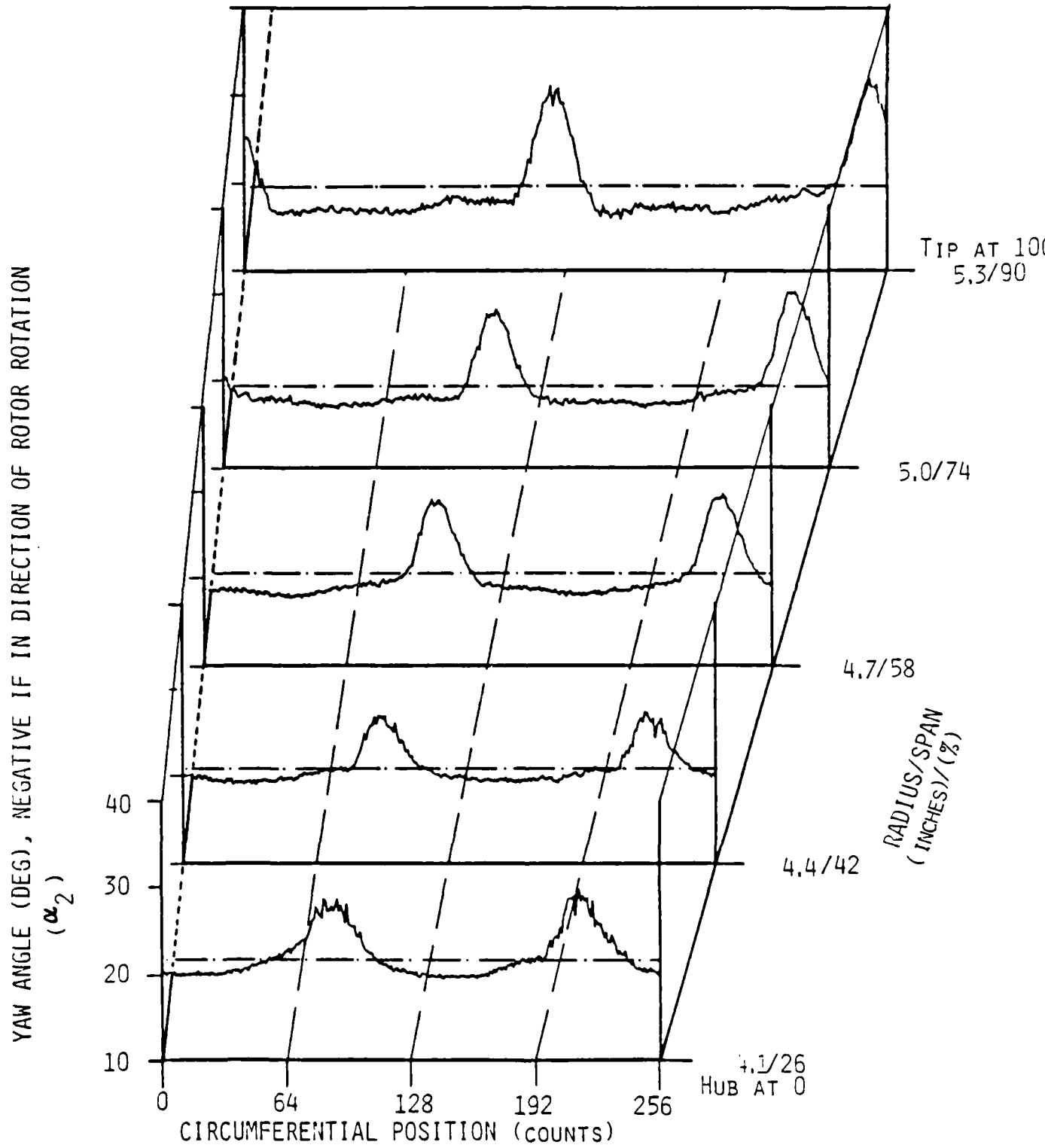

Figure 15b. DPDS Measurements of Blade-to- Blade Flow Yaw Angle

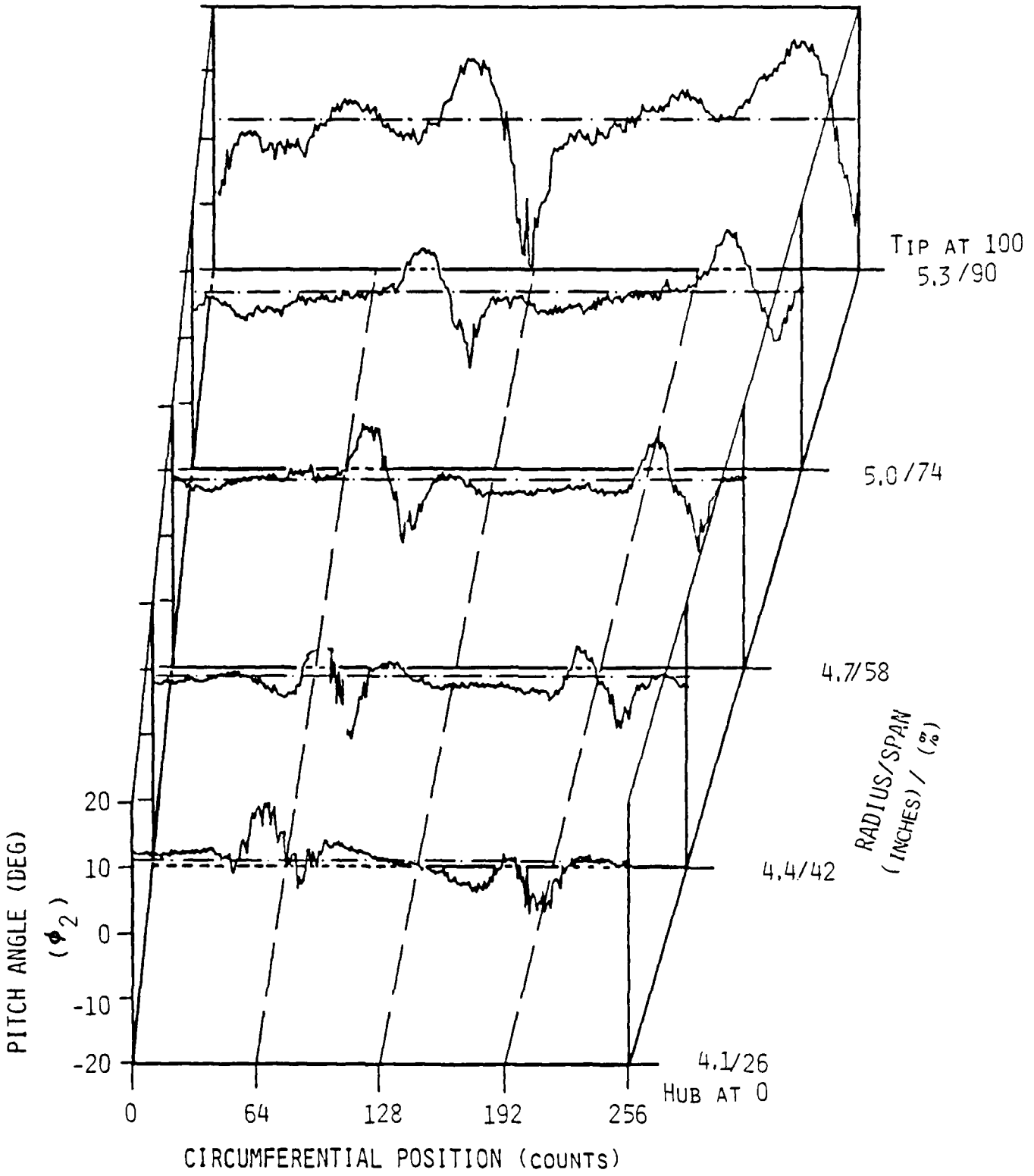

Figure 15c. DPDS Measurements of Blade-to-Blade Flow Pitch Angle

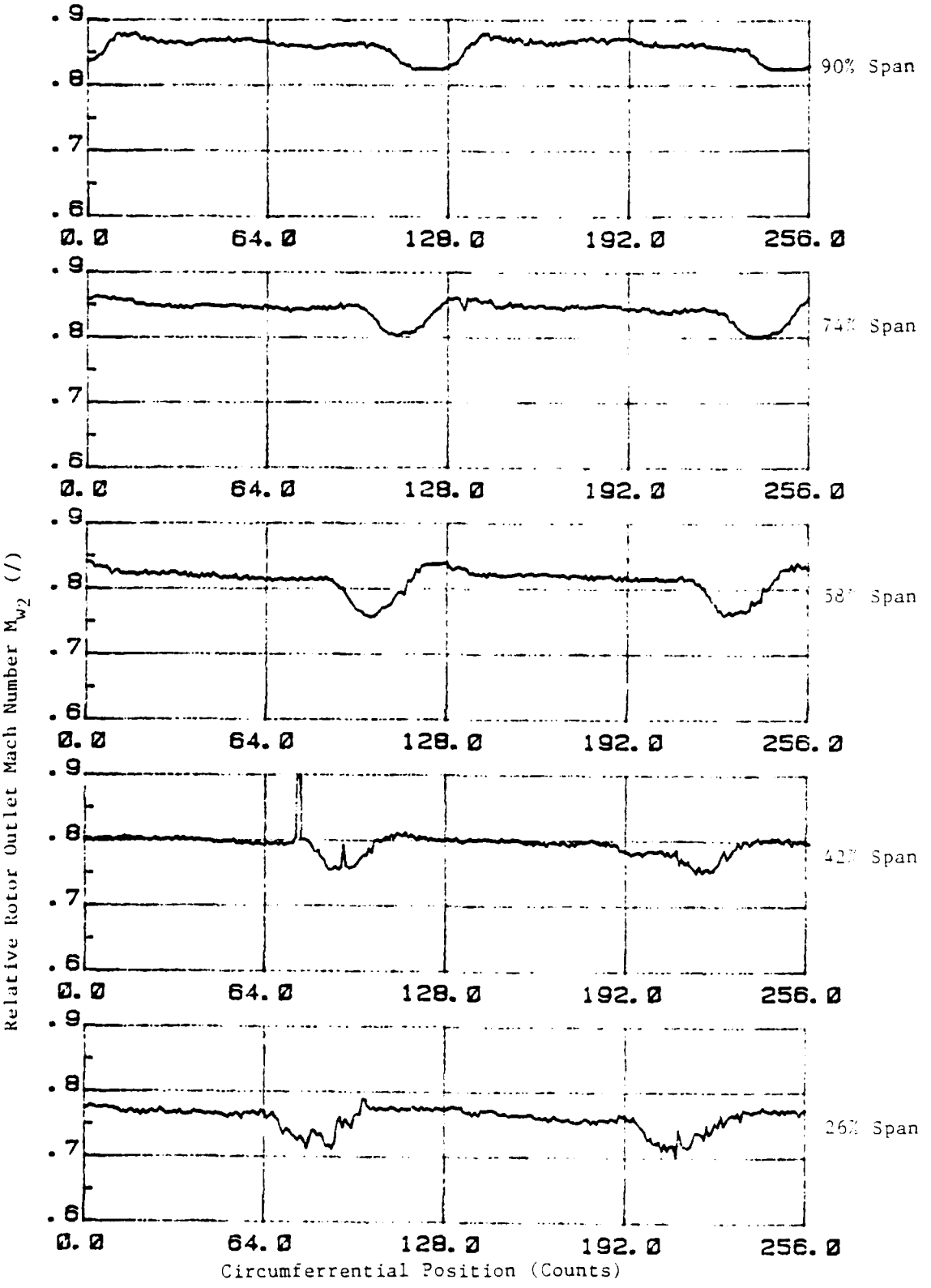

Figure 16. Relative Mach Number of Blade-to-Blade Flow

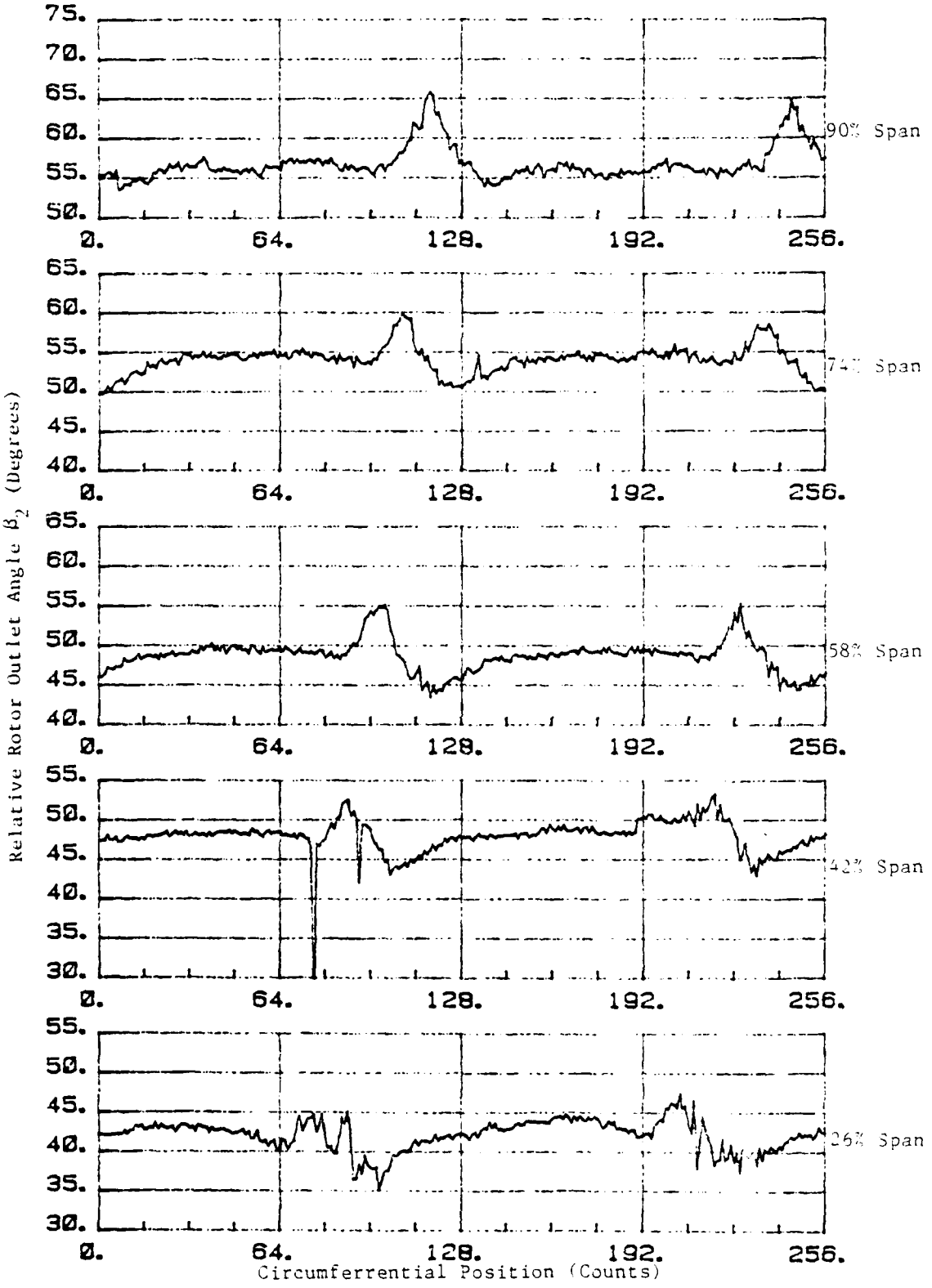

Figure 17. Relative Flow Angle Blade-to-Blade

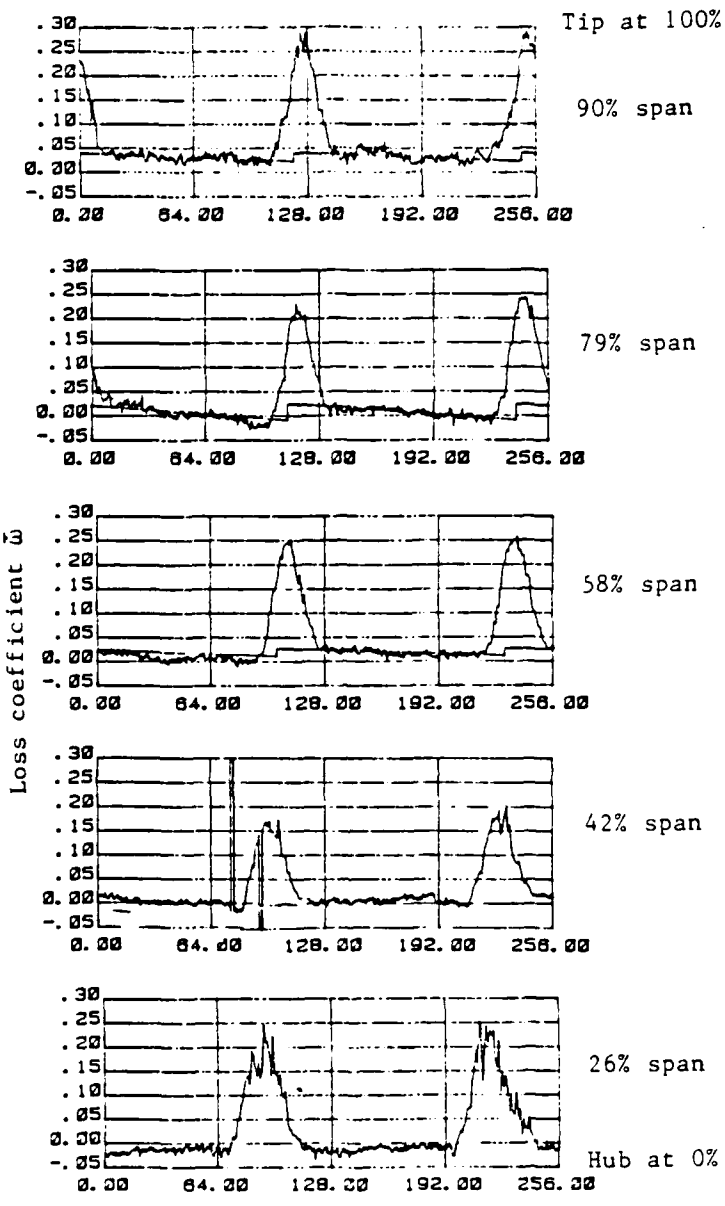

Figure 18. Measured Distribution of Loss Coefficient Blade-to-Blade

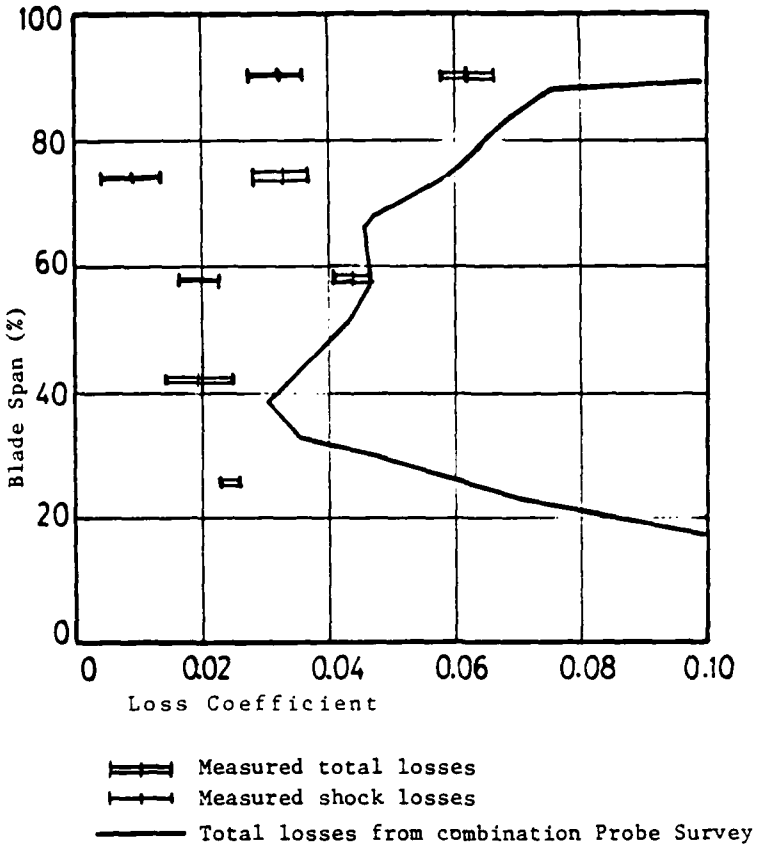

Figure 19. Distribution of Losses, Hub-to-Tip

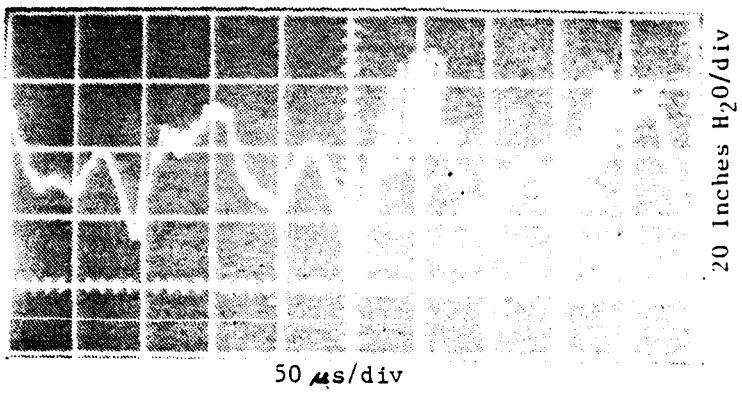

Figure 20. Example of Rotor-Tip Case-Wall Static Pressure Transducer Output

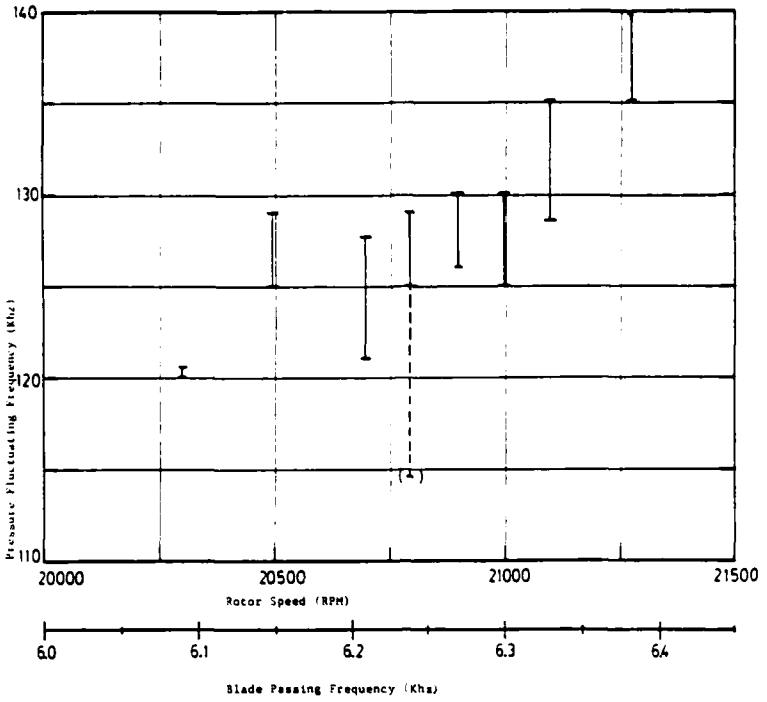

Figure 21. Measurements of the High Frequency Oscillation as a Function of Rotor Speed at Open Throttle

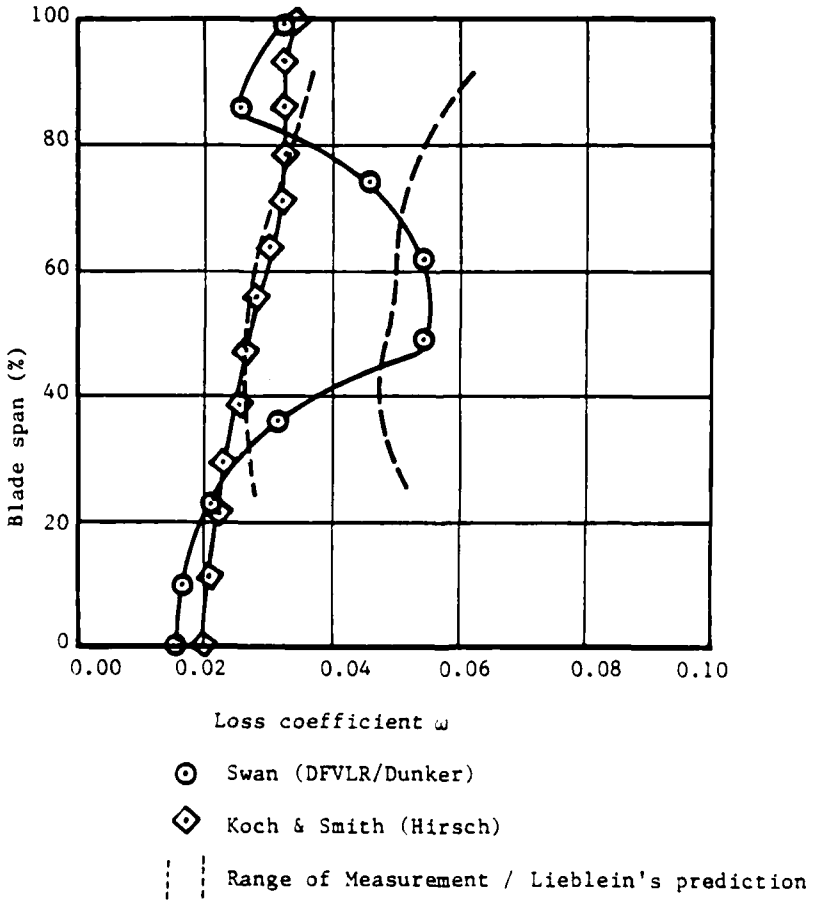

Figure 22. Profile Loss Distribution

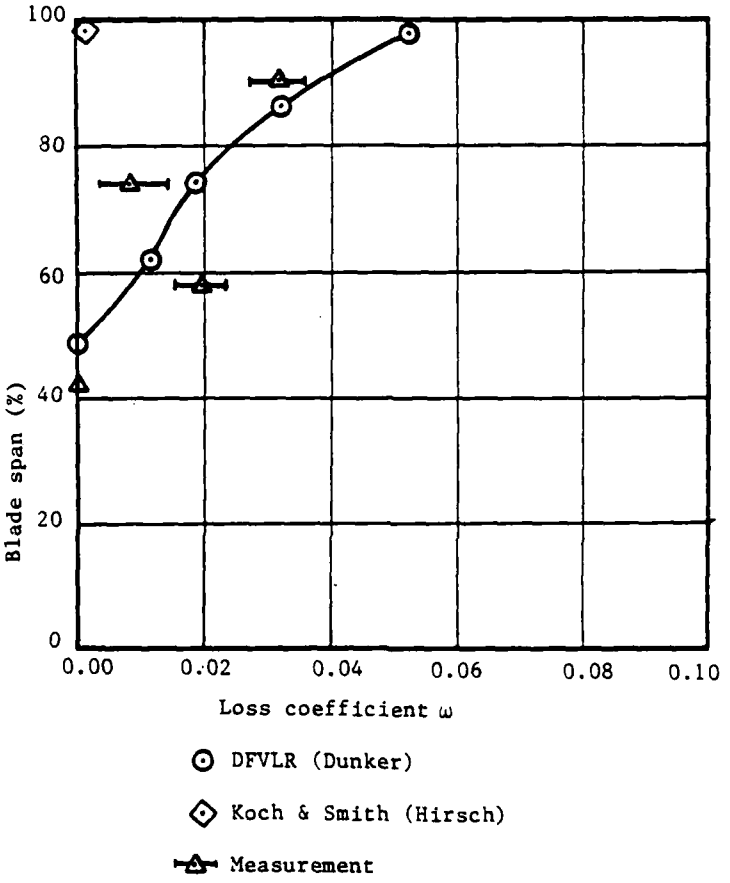

Figure 23. Shock Loss Distribution

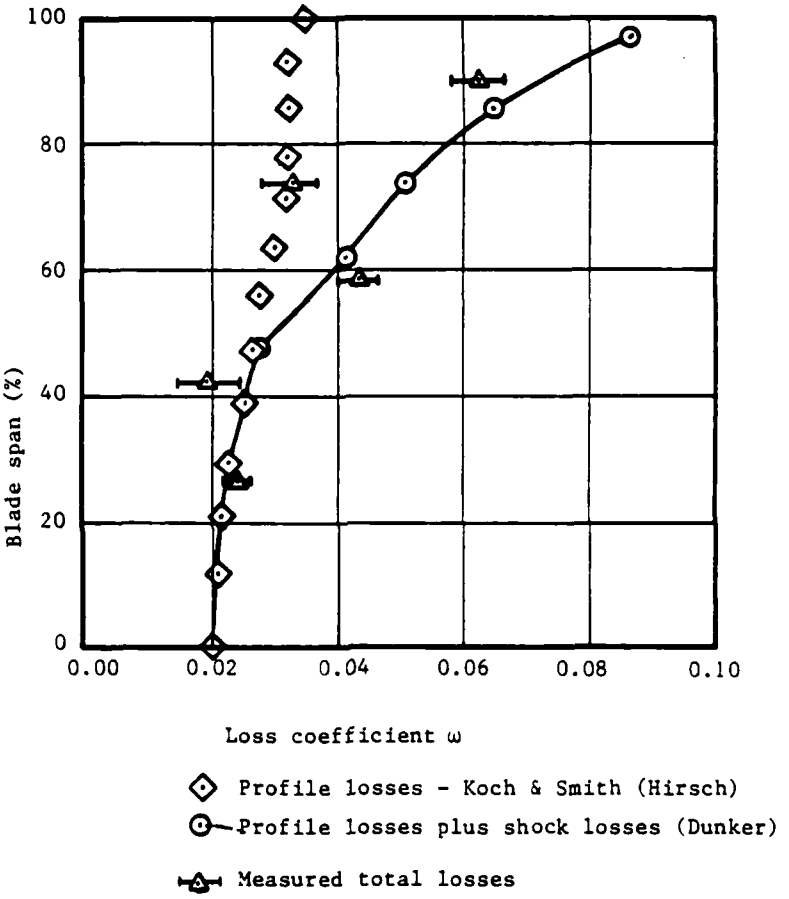

Figure 24. Comparison of Loss Measurements with Loss Models

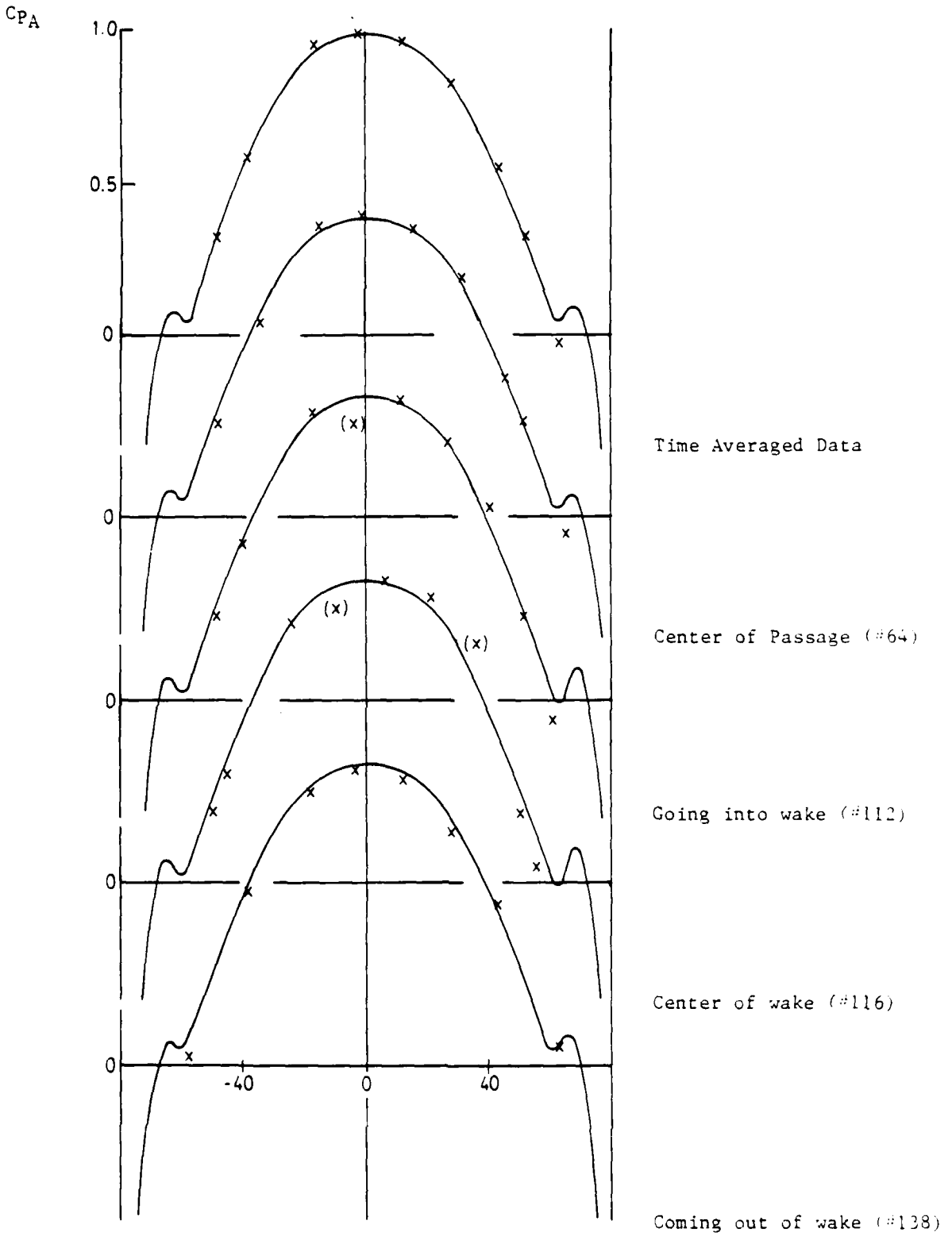

Figure 25. Pressure Coefficient versus Yaw Angle for Type A Probe at Various Positions Blade-to-Blade (x) Compared with Calibration

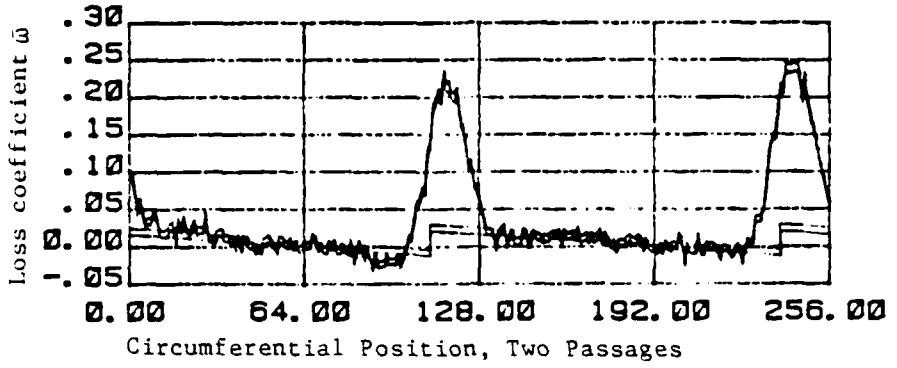

Figure 26. Uncertainty in Loss Coefficient Resulting from Measured Calibration Drift

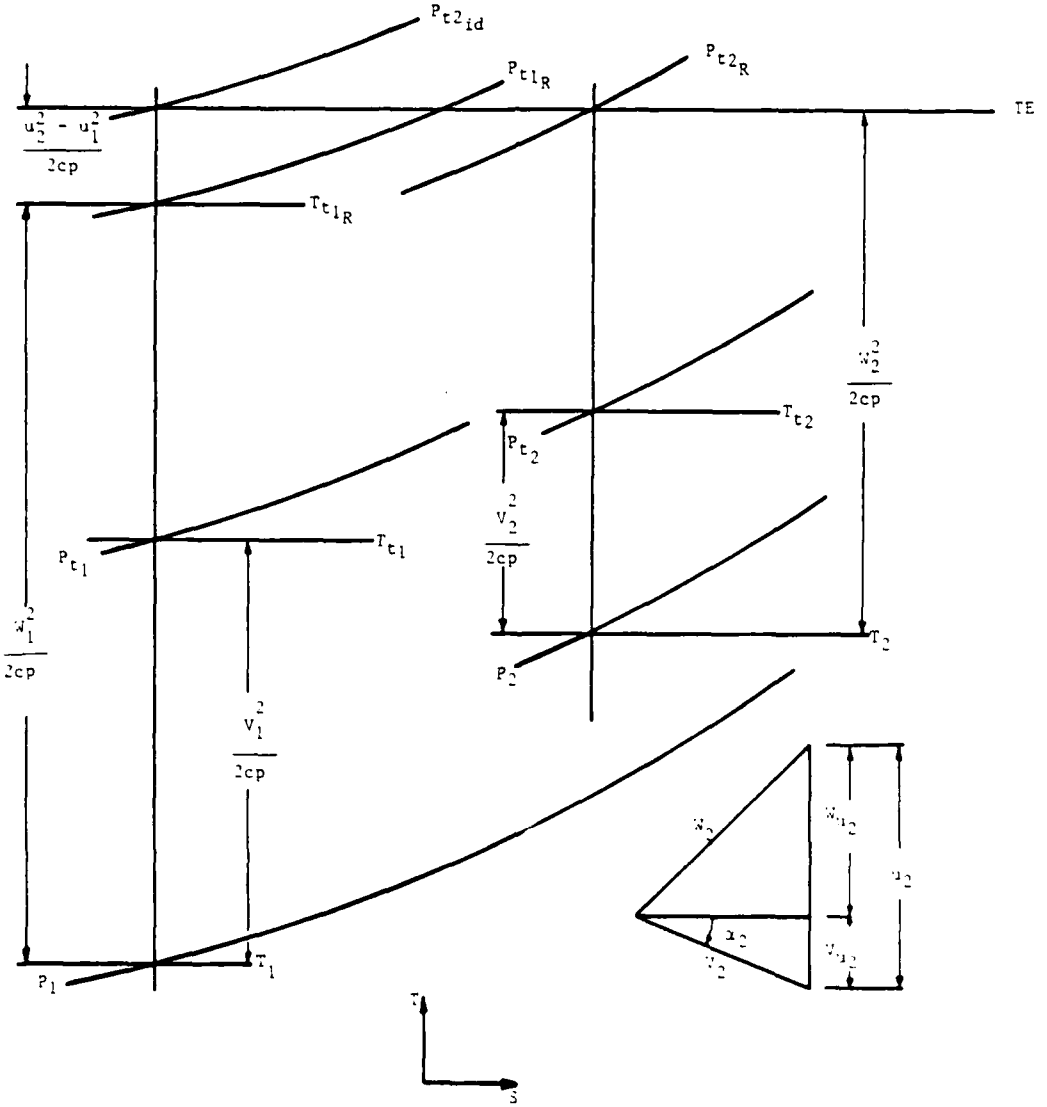

Figure 27. Temperature Entropy Diagram for Flow Through the Rotor

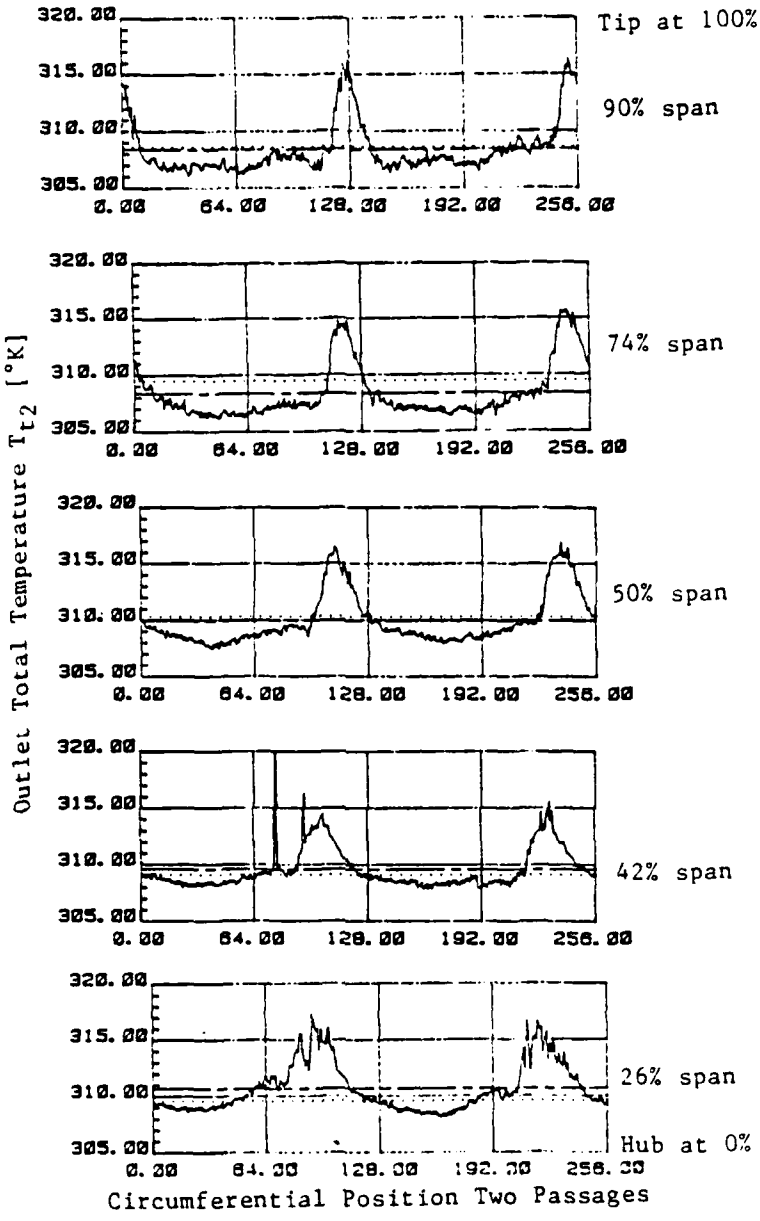

Dotted line - combination probe
(time-averaged reading)

Center line - mass averaged value
from distribution

Figure 28. Temperature Distribution, Blade-to-Blade
Derived from DPDS Measurements

APPENDIX A

ACCURACY OF THE RESULTS

A.1 COMBINATION PROBE

Possible measurement errors of the combination probe could influence the results in two ways. First, the rotor upstream conditions, which are used in the calculation of losses, depend on the accuracy of the combination probe. Second, the Kulite transducers used in the DPDS technique are calibrated on-line to equate the time-averaged measurement of the dual probe system to the combination probe measurements of the flow downstream of the rotor. Upstream of the rotor the combination probe is exposed to fairly low speeds in a steady environment only. It was shown in the probe calibration process (Ref 3), that under these circumstances the probe will resolve the velocity vector to better than 1% uncertainty. However, in the rotor outlet plane the probe is exposed to a velocity and associated pressure field, which fluctuates at blade passing frequency. In Ref 20 it is demonstrated, that a pneumatic probe will give an incorrect time-averaged pressure depending on the magnitude of pressure amplitudes and frequencies. For the probes used here, it was shown earlier (Ref 3), that the errors were negligible at rotor speeds up to 50% of design. The evaluation given in Ref 3 was repeated for conditions found in the present work at 70% speed and, because of the low amplitudes in the rotor wakes, the error was found again to be negligible.

A.2 VERIFICATION OF DPDS TECHNIQUE BY REDUNDANCY

In order to evaluate the accuracy of the DPDS results, use was made of the probe characteristics established in the calibration. If a pressure coefficient, C_{PI}, is defined as

$$C_{PI} = \frac{P_I - P_s}{P_t - P_s} \qquad A(1)$$

Where I is either A or B, depending on the probe, the dependences of C_{pI} on flow Mach number, yaw and pitch angle are established in the calibration. For any given combination of Mach number the dependence of C_{pI} on flow yaw angle is a unique characteristic of the probe. In the data reduction process only four discrete values of pressure from the 2 probes are used. To obtain those four values however, data for a range of probe yaw angle (9 settings) is acquired, since the local flow yaw angle is not known prior to the measurement. When the data is reduced, values for total and static pressure are obtained. Using these and equation A(1) the pressure coefficient C_{pI} can be defined for each of the measured pressures. Thus curves of C_{pI} versus probe yaw angle can be established for each point of measurement (256 blade-to-blade). If the resulting curves match those obtained in the steady-flow calibration at corresponding Mach numbers and pitch angles, the measurements are clearly valid. Since only four data values are needed to derive the velocity and flow angle magnitudes, the demonstration that the remaining data values from the probes are consistent with the derived magnitudes, provides multiply redundant verification of the measurements. In Fig 25 comparisons are shown between measurements taken with the Type A probe at 90% span and calibration curves at corresponding Mach numbers and pitch angles. The uppermost figure shows results from time-averaged measurements made with the dual-probe system. (At each angle setting, the DC outputs of the two probes were recorded and the data reduced to obtain the time-averaged velocity vector for the complete rotor, - a measurement which is equivalent to that made by the combination probe). The second figure is for data taken at position #64 which is in the center of the blade passage. The agreement between data and the probe characteristic calibration curve is good in both

cases. The lower three figures show results at locations going into (#112), at the center of (#116) and coming out of (#138) the rotor wake. In contrast to the results obtained with earlier probes (Ref 4), the agreement with steady state calibration characteristics is quite acceptable. The departures which are seen are isolated points and random in character. The skewing of the characteristic experienced in wake measurements made with the earlier probe tip (Ref 4), was not found with the present geometry shown in Fig 3 and Fig 4.

A.3 CALIBRATION DRIFT

In order to account for the temperature sensitivity of the Kulite transducers, the calibrations of the Type A and Type B probe transducers are performed on-line when test conditions have stabilized. The slopes of the transducers are obtained by applying known pressures to the reference side. The intercepts are derived by equating the time-averaged measurements of combination and dual probe systems. This procedure was carried out before and after the blade-to-blade data at nine angles were recorded. The average of the two calibrations was taken and the data set was rejected if the calibration drift exceeded 2% in slope or intercept. The uncertainty from averaging the two calibrations is shown in Fig 26 where data are shown at 74% span at 70% speed. The data were reduced using the first and second on-line calibrations. The values of both pitch and yaw angle were the same to better than .01°, the Mach number was changed less than 1% and the total pressure in the absolute frame changed less than 1.3%. While the distribution of losses blade-to-blade was little changed qualitatively, the magnitude of the mass-averaged value was increased or decreased about the mean value by approximately 8%. Similar changes were obtained in the computations of the shock loss. It is the uncertainty in the loss values due to the calibration uncertainty which is shown with the data in Fig 19, 23 and 24.

APPENDIX B

EVALUATION OF PARAMETERS IN THE RELATIVE FRAME

In order to compare the losses in the rotor to those in a two dimensional cascade, the losses in the relative frame of the rotor must be expressed in terms of the measurements which are made in the absolute frame. The losses are defined as

$$\bar{\omega} = \frac{\bar{P}_{t2_{Rid}} - P_{t2_R}}{\bar{P}_{t1R} - \bar{P}_1} \qquad B(1)$$

where id denotes ideal conditions as defined in the T-S diagram shown in Fig 27. The following derivations of pressures use non-dimensional velocities defined as

$$X_{u1} = \frac{U_1}{V_{t1}} \quad , \; X_{u2} = \frac{U_2}{V_{t1}} \quad , \; X_{v1} = \frac{V_1}{V_{t1}}, \; X_{v2} = \frac{V_2}{V_{t2}} \qquad B(2)$$

where V_{t1} and V_{t2} are the limiting velocities given by

$(V_t = \sqrt{2C_pT_t})$

From Fig 27 we obtain

$$\frac{P_{t2Rid}}{P_{t1}} = \left(\frac{T_E}{T_{t1}}\right)^{\gamma/\gamma-1} \qquad B(3)$$

and $$T_E - T_{t1} = \frac{1}{2cp} \left(W_1^2 + U_2^2 - U_1^2 - V_1^2\right) \qquad B(4)$$

Axial inflow results in $W_1^2 = U_1^2 + V_1^2$ B(5)

so that

$$P_{t2Rid} = P_{t1} \left(1 + X_{u2}^2\right)^{\gamma/\gamma-1} \qquad B(6)$$

P_{t1R} is calculated at constant entropy using

$$\frac{P_{t1R}}{P_{t1}} = \left(\frac{T_{t1R}}{T_{t1}}\right)^{\gamma/\gamma-1} \qquad B(7)$$

where

$$T_{t1R} - T_{t1} = \frac{1}{2cp}\left(W_1^2 - V_1^2\right) = \frac{U_1^2}{2cp} \qquad B(8)$$

so that

$$P_{t1R} = P_{t1} \left(1 + X_{u1}^2\right)^{\gamma/\gamma-1} \qquad B(9)$$

P_1 is given by

$$P_1 = P_{t1} \left(1 - X_{v1}^2\right)^{\gamma/\gamma-1} \qquad B(10)$$

In equations B(6), B(7) and B(10) the measured (constant) time - average quantities of P_{t1}, X_{u1}, X_{u2} and X_{v1} are used. $\overline{P}_{t2id}$, $\overline{P}_{t1R}$ and $\overline{P}_1$ are taken to be constant peripherally, while P_{t2R} varies blade-to-blade.

From Fig 27

$$\frac{P_{t2R}}{P_{t2}} = \left(\frac{T_E}{T_{t2}}\right)^{\gamma/\gamma-1} \qquad B(11)$$

and

$$\frac{T_E}{T_{t2}} = \left(T_E - T_{t2}\right)\frac{1}{T_{t2}} + 1 \qquad B(12)$$

From Fig 27

$$T_E - T_{t2} = \frac{1}{2cp}(W_2^2 - V_2^2) = \frac{1}{2cp}(W_{u2}^2 - V_{u2}^2) \qquad B(13)$$

and, rewriting

$$T_E - T_{t2} = \frac{1}{2cp}(W_{u2}^2 + 2W_{u2}V_{u2} + V_{u2}^2 - 2W_{u2}V_{u2} - 2V_{u2}^2) \qquad B(14)$$

From the velocity triangle

$$T_E - T_{t2} = \frac{1}{2cp}(U_2^2 - 2V_2U_2 \sin\alpha_2) \qquad B(15)$$

so that

$$\frac{T_E}{T_{t2}} = \frac{1}{2cpT_{t2}}(U_2^2 - 2V_2U_2 \sin\alpha 2) + 1 \qquad B(16)$$

or

$$\frac{T_E}{T_{t2}} = X_{u2}^2 \frac{T_{t1}}{T_{t2}} - 2\sin\alpha_2 X_{v2} X_{u2}\sqrt{\frac{T_{t1}}{T_{t2}}} + 1 \qquad B(17)$$

Using Eq B(11),

$$P_{t2R} = P_{t2}\left(X_{u2}^2 \frac{T_{t1}}{T_{t2}} - 2\sin\alpha X_{v2} X_{u2}\sqrt{\frac{T_{t1}}{Tt2}} + 1\right)^{\gamma/\gamma-1} \qquad B(18)$$

To calculate $P_{t_{2R}}$ from measurements, the individual readings of P_{t2}, α_2 and X_{v2} blade-to-blade have to be taken from the DPDS data, while Xu_2 and T_{t1}/T_{t2} are average quantities.

In Eq B(17), writing

$$\frac{T_E}{T_{t2}} = \frac{T_{t1}}{T_{t2}} \cdot \frac{T_E}{T_{t1}} = X_{u2}^2 \frac{T_{t1}}{T_{t2}} - 2\sin\alpha_2 X_{v2} X_{u2} \sqrt{\frac{T_{t1}}{T_{t2}}} + 1$$

then

$$\frac{T_{t1}}{T_{t2}} \left(\frac{T_E}{T_{t1}} - X_{u2}^2\right) + \sqrt{\frac{T_{t1}}{T_{t2}}} 2X_{v2} X_{u2} \sin \alpha_2 - 1 = 0 \qquad B(19)$$

Using Eq B(4) and Eq B(6), Eq B(19) becomes

$$\frac{T_{t1}}{T_{t2}} + \sqrt{\frac{T_{t1}}{T_{t2}}} 2X_{v2} X_{u2} \sin\alpha_2 - 1 = 0 \qquad B(20)$$

The total temperature ratio across the rotor can thus be written as a distribution blade-to-blade in terms of velocities as

$$\sqrt{\frac{T_{t1}}{T_{t2}}} = X_{v2} X_{u2} \sin\alpha_2 \pm \sqrt{X_{v2}^2 X_{u2}^2 \sin^2\alpha_2 + 1}$$

From the DPDS technique the values of X_{v2} and α_2 are known blade-to-blade, while X_{u2} is constant. Figure 28 shows the distribution of total temperature blade-to-blade for one set of data obtained at the rotor outlet. The mass averaged temperature from the distribution is shown in comparison to the measured average temperature.

REFERENCES

1. Neuhoff, F., "Investigation of the Interaction between Rotor and Stator of a Transonic Compressor,"Naval Postgraduate School, Monterey, CA, November 1985, Under Contract N62271-85-M-0423.

2. Erwin, J. R., "A Review of the Design of the NPS/TPL Transonic Compressor," Naval Postgraduate School, Monterey, CA, (NPS67-83-004CR), 1983.

3. Neuhoff, F., "Calibration and Application of a Combination Temperature-Pneumatic Probe for Velocity and Rotor Loss Distribution Measurements in a Compressor," BMD Corporation, Monterey, CA, (NPS67-81-03CR), December 1981.

4. Shreeve, R. P, Neuhoff, F., "Measurements of the Flow From a High-Speed Compressor Rotor Using a Dual Probe Digital Sampling (DPDS) Technique," (ASME 83 GT-215), Naval Postgraduate School, Monterey, CA, April 1984.

5. Neuhoff, F., "Further Development of a Dual-Probe Digital Sampling (DPDS) Technique For Measuring Flow Fields in Rotating Machines," BDM Corporation, Monterey, CA, (NPS67-82-01CR), September 1982.

6. Hirsch, IR., C., "Computer Program for Turbomachinery Flows Finite Element Method General Principles," Vrije Universiteit, Brussels, Belgium, 1981.

7. Hirsch, IR., C., "Computer Program for Turbomachinery Flows Finite Element Method User's Guide," Vrije Universiteit, Brussels, Belgium, 1981.

8. Neuhoff, F., "Modifications to the Inlet Flow Field of a Transonic Compressor Rotor," TR 8503, Naval Postgraduate School, Monterey, CA, (N62271-85-M-0423.

9. Scholz, I. N., "Aerodynamik der Schaufelgitter Band I," Verlag G. Braun Karlsruhe, 1965.

10. Schreiber, H. A., DFVLR, "Experimentelle Untersuchung des Verdichtergitters LO30-4 mit Variation des axialen Massenstromdichteverhaltnisses im transsonischen Machzahlbereich," IB 325/4/1981, September 1981.

11. Ng, W. F., Epstein, A. H., "Unsteady Losses in Transonic Compressors," (ASME 84-GT-183), Massachusetts Institute of Technology, 1984.

12. Strazisar, A. J., "Investigation of Flow Phenomena in a Transonic Fan Rotor using Laser Anemomentry," NASA-Lewis Research Center, Cleveland, OH, 1984, ASME Gas Turbine Conference, Amsterdam.

13. AGARD Advisory Report No. 175, "Through Flow Calculations in Axial Turbomachines, Part II, Axial Compressor Performance Predictions," October 1981.

REFERENCES

14. Lieblein, Schwenk, F. C., Broderick, R. L., "Diffusion Factor for Estimating Losses and Limiting Blade Loadings in Axial-Flow-Compressor Blade Elements," NACA RM E53D01.

15. Dunker, R., "Untersuchungen zur Weiterentwicklung der Kennfeldberechnungsverfahren fur transsonische Axialverdichter," Abschlussbericht, DFVLR IB 325/5/1981, July 1981.

16. Swan, W. C., "A Practical Method of Predicting Transonic-Compressor Performance," Transaction of the ASME Journal of Engineering for Power, Vol. 83, No. 3, July 1961, page 322.

17. Koch, C.C., Smith Jr., L. H., "Loss Sources and Magnitudes in Axial-Flow Compressors," Transaction of the ASME Journal of Engineering for Power, July 1976, page 411.

18. Melzer, T., "Vorausberechnung des Betriebsverhaltens einer axialen Transonikverdichterstufe," M.S. Thesis, Hochschule der Bundeswehr Munchen, West Germany, October 1984.

19. Moeckel, W. E., "Experimental Investigation of Supersonic Flow with Detached Shock Waves for Mach Numbers between 1.8 and 2.9," NACA RM E50D05, 1950.

20. Weyer, H., "The Determination of Time-Weighted Average Pressures in Strongly Fluctuating Flows, Especially in Turbomachines," DFVLR 74-34, 1974.

END

FILMED

5-86

DTIC